

Research Paper

Dispersions of carbon nanotubes by helical flavin surfactants: Solvent induced stability and chirality enrichment, and solvatochromism

In-Seung Choi, Minsuk Park, Eunhye Koo, Sang-Yong Ju*

Department of Chemistry, Yonsei University, Seoul, 03722, Republic of Korea

ARTICLE INFO

Article history:

Received 19 June 2021

Received in revised form

9 August 2021

Accepted 18 August 2021

Available online 20 August 2021

Keywords:

Single-walled carbon nanotube

Dispersion

Solubility parameter

Chirality selection

Solvatochromism

Photoluminescence quantum yield

ABSTRACT

Although solvent governed stability, selection and optical behavior of single walled carbon nanotubes (SWNTs) brought about by using specialized surfactants have importance in relation to various opto-electronic and biological applications, their origins and solvatochromism have not been thoroughly explored owing to the lack of ideal surfactant dispersing SWNTs. We show that solvent driven SWNT selection and solvatochromism occurs in SWNTs wrapped by two flavin derivatives in solvents with dielectric constants (ϵ) ranging from 2.3 to 80.4. Flavin-SWNT nanocomposite dispersions exhibit near-armchair and chirality-specific enrichment in lower ϵ aromatic solvents, and those with broader chirality selectivity are formed in higher ϵ solvents. Those trends are also observed by controlling flavin concentration. Consideration of optical spectra provides relative quantum yields of flavin-SWNT in each solvent, showing toluene and *p*-xylene dispersions as best owing to highly individualized SWNT. The selectivities and relative stabilities of the flavin-SWNT nanoconjugates are associated with the solubility parameter (δ), which controls the respective morphology of the side chains and the relative Gibbs energies of the nanoconjugates relative to those of the free flavin and SWNTs. Differences between δ of side chains vs. the media results in extended and collapsed side chain conformations in respective lower and higher ϵ solvents, leading to diameters (d_t) selection of SWNT owing to diameter modulation of the isoalloxazine assembly. In addition, with increasing ϵ optical transitions of flavin/SWNT exhibit lower bathochromic shifts owing to a passivating role played by the isoalloxazine that does not take place with other surfactants. The results suggest new guidelines for the design of good SWNT dispersions that take into consideration self-association of the surfactant, conformations of side chains and the nature of the solvent.

© 2021 Elsevier Ltd. All rights reserved.

1. Introduction

Modulation of the optical properties of single walled carbon nanotube (SWNT) and especially its near-infrared (NIR) optical transitions [1,2] governed by a chiral vector defined by (n, m) has drawn attention. The excited state properties of SWNT are governed by strongly bound electron-hole pairs through Coulombic interactions. Excitonic modulation of individualized semiconducting SWNT enables potential applications in photovoltaics [3,4], thin-film transistors [5,6], sensors [7], and bio-imaging [8,9] and biomarker [10,11] systems. However, SWNT has a high propensity to undergo bundling owing to surface energy and solubility. As a result, a fundamental understanding of its excitonic properties

hinges on the ability to bring about individualization of SWNT using surfactants and various media [2]. Therefore, surfactants and media play paramount roles in determining the local environments of SWNT and, consequently, they impact the excitonic behavior of this material.

In this context, ideal SWNT dispersions contain stable and highly individualized SWNT (iSWNT) that is not contaminated by bundled SWNT (bSWNT), a carbonaceous impurity (CI) and metal catalyst impurities. Owing to their relatively high mass, metallic impurities can be easily removed by using benchtop centrifugation. The degree of individualization of SWNT dispersions [12], generated by using selected aromatic surfactants that possess alkyl terminal groups (*i.e.*, poly(fluorene) [13–15], poly(thiophene) [16] and *N*-dodecyl flavin (FC12) [5,12]), is solvent polarity dependent. Specifically, highly iSWNT dispersions are formed in aromatic solvents (*i.e.*, toluene) that have low dielectric constants (ϵ), whereas bSWNT dispersions predominate in solvents having higher ϵ . For

* Corresponding author.

E-mail address: syju@yonsei.ac.kr (S.-Y. Ju).

example, a dioctyl poly(fluorene) dispersion in toluene [13–15] contains highly iSWNTs with minimized background absorption resulting from bSWNT and CI [17–19]. Moreover, this dispersion displays near armchair chirality selection in which n and m values in the (n, m) chiral vector are similar. This selectivity for enrichment of high purity semiconducting SWNT has proven to be useful for use in various high-end electronic applications [3–11]. Therefore, understanding of possible solvent-specific chirality selections of SWNT [20] by using a single surfactant requires knowledge about the general trends in various solvents.

Optical transitions in SWNT undergo solvent dependent shifts, a phenomenon known as solvatochromism [21,22]. An example of the solvatochromic behavior of bare SWNTs is the simultaneous bathochromic shifts taking place in first (e_{11}^S) and second (e_{22}^S) semiconducting excitonic transitions as the ϵ value of the solvent is increased [23]. Despite its importance, solvatochromism of aqueous surfactant-wrapped SWNTs has received limited study with attention being given only to microenvironments between SWNT and surfactant by which organic solvents are encapsulated [24,25]. Surfactant rigidity also affects the excitonic decay behavior of SWNT. For example, reorganizable sodium dodecyl sulfate (SDS) wrapping induces much faster exponential decay components than does wrapping with rigid sodium cholate [26], underscoring the importance of surfactant organization. Especially, the lack of surfactant which disperses SWNT in various organic/aqueous solvents necessitates the use of solvent cocktails, to induce solvatochromic shift of SWNT, which further obscures the homogeneity of solvents near surfactant/SWNTs [27,28]. Because of the lack of full characterization of surfactant structures [29,30], a limited understanding exists for the effects of solvents on SWNT properties.

Flavin mononucleotide (FMN, Fig. 1A) and *N*-dodecyl flavin (FC12) have preferential affinities for SWNT [12,31–35]. FMN utilizes helical wrapping motifs (Fig. 1B) to stabilize SWNTs [32,36] through π - π interaction between the flavin isoalloxazine ring and graphene sidewalls, quadruple hydrogen-bonding (H-bonding) between adjacent uracil moieties within the isoalloxazine ring which aligns along longitudinal direction of SWNT, and anionic dispersion promoted by the monosodium form of the *d*-ribityl phosphate side chains. FMN [32,37] and FC12 [38] also promote preferential self-organization of specific SWNT chirality (*i.e.*, (8,6)). Furthermore, FC12 selectively disperses semiconducting SWNT with a greater than 90% purity and it enables the formation of high performance thin film transistors [5]. In addition, as compared to other widely used surfactants (*i.e.*, SDS and sodium cholate), flavins engage in tight helical wrapping that has higher resistance to covalent functionalization of SWNT by reactions with diazonium salts [37]. The unique features of the isoalloxazine ring not only leads to stabilization of SWNT, but it also induces stabilization of multi-

walled carbon nanotube [39,40], graphene [41,42] and hexagonal boron nitride [43]. Importantly, unlike polymeric surfactants, small molecules like FMN and FC12 are advantageous for facile chemical modifications [4,44] and suitable for high-end applications.

In the investigation described below, we explored the dispersion stability, chirality selection and optical behavior of SWNT wrapped by isoalloxazine derivatives in various solvents with various ϵ values in the 2.27 to 80.4 range. In the effort, we first examined the absorption and photoluminescence (PL) properties of isoalloxazine/SWNT systems in solvents having varying ϵ , in which the origin of background absorption and relative photoluminescence quantum yield (Φ_R) have been addressed using various methodologies. Next, consideration was given to how the solubility parameter (δ) of the flavin side chain affects the nature of the SWNT dispersion. Thirdly, we probed the solvatochromism of isoalloxazine/SWNT dispersion and compared it to that of SWNT stabilized by other surfactant system in the context of assessing the effect of charge transfer.

2. Results and discussion

2.1. Optical transitions of isoalloxazine-wrapped SWNT dispersions in various solvents

FC12 was synthesized using the previously reported procedure [5,12], and commercially available FMN was used in the monosodium salt form. The two flavin derivatives were used as surfactants to disperse SWNT in various organic solvents and water, respectively. To prepare dispersions, HiPco SWNT with a d_t distribution of 1.0 ± 0.3 nm was subjected to sonication in isomolar surfactant solution in solvent with various ϵ values. Especially, the ratio of components, namely 1:4:4 protocol (*i.e.*, 1 mg HiPco, 4 mL solvent, and 4 mg FC12 in that order) was representatively selected because flavins have different binding affinities and enrichment with SWNT that depend on the flavin/SWNT weight ratio [45]. This ratio was used for procurements of UV–vis–NIR absorption spectra and photoluminescence excitation (PLE) maps from the SWNT dispersions (see Methods). In addition, possible pH-induced absorption changes in FMN-SWNT dispersion (*i.e.*, pH = 4.0, 7.0, and 10.0) were tested and shown to be negligible (Fig. S1 of Supplementary Information (SI)). This finding suggests that flavin coating effectively prevents acid-induced photobleaching, which is prevalent in loosely packed SDS wrapped SWNT [46]. This result suggests that flavin wrapping is tight enough to exclude doping effects by solvents, as has been reported earlier [37].

The results show that the absorptions and PL properties of the flavin-SWNT dispersions differ depending on the ϵ values of solvents over a wide range from 2.27 to 80.4 (*i.e.*, *p*-xylene, benzene,

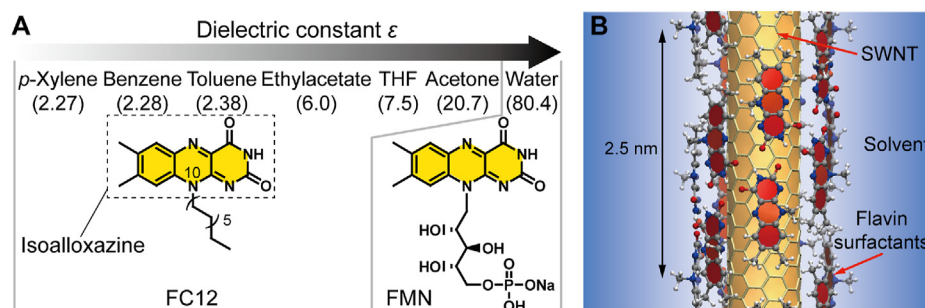


Fig. 1. Dispersions of SWNT by two flavin derivatives FC12 and FMN in various solvents. (A) Top: list of solvents capable of dispersing SWNT individually and their ϵ values. Bottom: structures of FC12 and FMN, in which the isoalloxazine ring is highlighted and partial IUPAC numbering of isoalloxazine ring is given. (B) Schematic illustration of SWNT (gold shade) wrapped by helical *N*-methyl isoalloxazine (lumiflavin, red shade) moieties which is used instead of FC12 and FMN for visual clarity. H, C, N, and O are colored in white, gray, blue, and red, respectively. (A colour version of this figure can be viewed online.)

toluene, ethyl acetate, tetrahydrofuran (THF), and acetone for FC12-SWNT dispersions, and water for FMN-SWNT dispersions). Fig. 2A and B shows normalized UV–vis–NIR absorption spectra and corresponding PLE contour maps of flavin-SWNTs obtained using the 1:4:4 protocol in seven solvent dispersions. For PL measurements,

dispersions were diluted to have eS22 absorbance below 0.05 to minimize self-absorption, and quantify Φ_R (discussed in the later section). Similar absorption spectra and PLE maps from dispersions with lesser (1:4:1 protocol) or greater amounts (1:4:8 protocol) of flavins are also presented for comparison purposes in Fig. 2C–F.

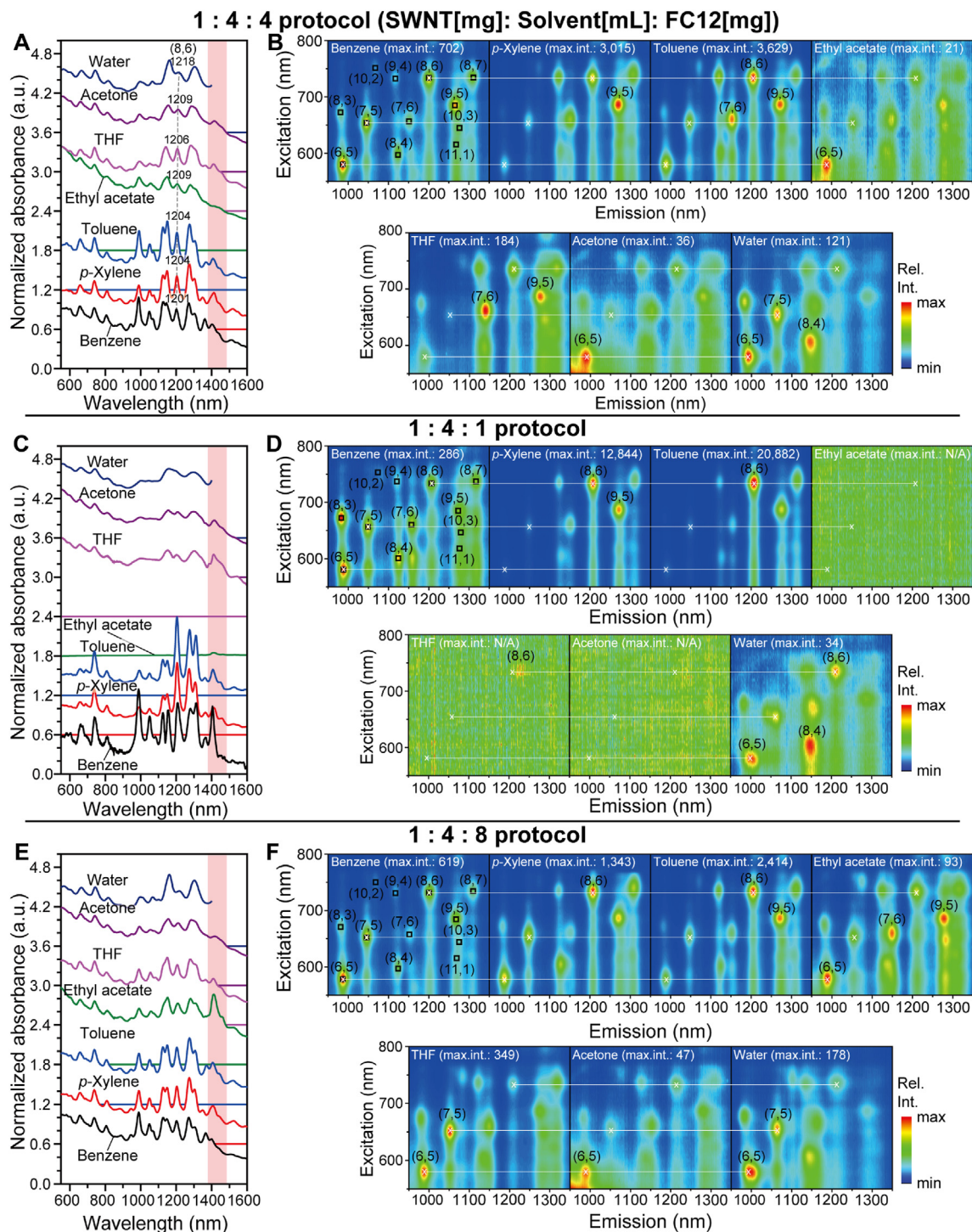


Fig. 2. Absorption spectra and PLE maps of flavin-SWNT dispersed in various solvents with various protocols. Data set from 1:4:4 protocol: (A) Normalized UV–vis–NIR absorption spectra of FC12-SWNT dispersions in organic solvents and a FMN-SWNT dispersion in water. Normalizations were conducted with respect to the absorbance maximum of $e^{S_{11}}$ near 1270 nm. Each spectrum is offset by 0.6 with increasing ϵ for visual clarity. Pink shaded area contains absorption from residual water. (B) Corresponding PLE contour maps of SWNT dispersions in various solvents. Rectangular symbols in the first panel indicate crosspoints of $e^{S_{11}}$ and $e^{S_{22}}$. White lines are drawn for the positional comparison of each $e^{S_{11}}$ and $e^{S_{22}}$. Several enriched species are denoted by (n, m) chiralities. Similar (C) absorbance and (D) PLE maps from dispersions with 1:4:1 protocol. Similar (E) absorbance and (F) PLE maps from dispersions with 1:4:8 protocol. (A colour version of this figure can be viewed online.)

When lesser amounts of FC12 are employed in the protocol (Fig. 2C and D), several high ϵ solvents (i.e., ethyl acetate, THF, and acetone) do not produce stable SWNT dispersions. With greater amounts of flavin, stable dispersions are formed from various solvents, displaying the respective absorption and PLE maps given in Fig. 2E and F. When compared with the solubilities of FC12 in various solvents (Table S1), these observations indicate that solvents having high solubilities with FC12 are inferior for generating dispersions with PL activities.

A comparison of the normalized absorption spectra (Fig. 2A, against *ca.* 1270 nm band) show that, among the dispersions, those in aromatic solvents display sharp e_{22}^S and e_{11}^S originating from SWNT chiralities. The absorption spectra in various solvents contain well resolved e_{22}^S (600–850 nm) and e_{11}^S (950–1550 nm) bands associated with various chirality distributions of HiPco SWNT [1,2]. In accord with previous findings [12], absorption bands of dispersions in lower ϵ aromatic solvents (i.e., *p*-xylene, benzene, and toluene) exhibit narrower full width at half maximum (Γ) for the e_{11}^S and e_{22}^S bands and lower background absorption (see Figs. S2A–F in SI for original absorption spectra (left) and their dilutions (right) of as-prepared dispersions from each protocol). Upon increasing ϵ , a simultaneous bathochromic shift and peak broadening of e_{11}^S and e_{22}^S bands occur along with an increase in background absorbance. It is well-known that background absorption originates from contributions from bSWNT and CI [17–19]. For instance, the e_{11}^S of isolated (8,6) SWNT shifts from 1201 nm to 1218 nm (dashed line in Fig. 2A) when the solvent's ϵ value increases. The overall change corresponds to a 14 meV bathochromic shift. In addition, increasing flavin concentrations (Fig. 2C, A and E) result in broader chirality distributions, evident by broader e_{11}^S chiralities absorption. Moreover, inspection of spectra (Figs. S2A, C, and E) shows that in higher ϵ solvents as-prepared dispersions display relatively higher background absorption as compared to e_{11}^S and e_{22}^S bands, suggesting that these solvents are more capable of dispersing bSWNT and CI which is sp^2 and sp^3 hybridized globular structure [17–19].

PLE contour maps obtained by varying solvents and flavin concentrations are useful in identifying of chiralities and their abundance of iSWNTs [2]. Inspection of these maps shows the existence of interesting trends according to varying flavin concentration and solvents. First, analysis of PLE maps using the 1:4:1 protocol (Fig. 2D) shows that toluene and *p*-xylene dispersions have enriched (8,6), and (9,5) SWNT species. In addition, increasing flavin concentrations (Fig. 2B and F) results in broadened chirality distribution towards smaller d_t SWNT, on top of (8,6) and (9,5) enrichments. Although benzene dispersions appear similar chirality distributions regardless of flavin concentrations, benzene dispersion prepared by much smaller flavin concentration (1:4:0.5 protocol) shows several chirality enrichments (i.e., (9,5) and (8,7)) in PLE map (Fig. S3B). Other solvents exhibit similar enrichment trends like *p*-xylene and toluene. In case of ethyl acetate, 1:4:4 protocol displays enriched (6,5) chirality and 1:4:8 protocol exhibits much broadened chirality selections (i.e., (6,5), (7,6), and (9,5)). In case of THF, while 1:4:4 protocol displays initial larger d_t enrichment centered on (7,6) and (9,5), 1:4:8 protocol shows smaller d_t enrichment near (6,5) and (7,5) chiralities. Similarly, acetone and water dispersions display enrichment trends toward (6,5) tubes with increasing flavin concentrations. Overall, although the selected chiralities of SWNT are different for each solvent, increasing flavin concentration results in deviation of near armchair chirality selection, less chirality-specific selection of SWNT, and broadening of chirality distribution towards smaller d_t SWNT. Especially, the (8,6) and (9,5) enrichments in toluene and *p*-xylene originate from the preferential binding affinity of the isoalloxazine supramolecular helical assembly, which possesses a

similar d_t to that of the SWNT (d_t (8,6) = 0.97 nm and d_t (9,5) = 0.98 nm) [32,38].

Another point to address is whether metallic contents of SWNT change during chirality enrichment of semiconducting SWNT prompted by either low ϵ solvents or lower flavin concentration. For this, absorption spectra containing the first optical transitions of metallic SWNT (e_{11}^M , 450–600 nm) of HiPco SWNT [47] were compared according to varying flavin concentrations. Fig. S4 shows absorption spectra changes of FC12-HiPco dispersions in *p*-xylene with increasing FC12 concentrations. Although e_{11}^M transitions smaller than 520 nm was masked by absorption tail of FC12 [5], e_{11}^M transition intensities gradually reduce as decreasing FC12 concentration and show minimum from 1:4:1 and 1:4:0.75 protocols.

The above results suggest that stoichiometry or the ratio of the isoalloxazine footprint area [48,49] on the outer SWNT surface area plays an important role for selection of certain SWNT chiralities. Previous molecular mechanics simulation results suggests that the isoalloxazine ring forms a self-assembled helix (Fig. 1B) which has 8₁ helix motif in which 16 isoalloxazine rings have equivalent surface area on 2.5 nm long (8,6) SWNT that contains *ca.* 290 carbons in the same longitudinal length [32,38]. This finding suggests that considering molecular weight of isoalloxazine ring (i.e., 241.07 g/mol) and assumption that all flavin exists on SWNT, 2 mg of FC12 has a surface area that is equivalent to 1 mg of SWNT with average d_t = 1.0 nm. In case of the 1:4:1 protocol, the overall footprint area of the used FC12 is smaller than that of the SWNT surface area, leading to binding-affinity driven selection of specific SWNT chiralities (i.e., (8,6) and (9,5)) [32]. In case of the 1:4:4 and 1:4:8 protocols, the overall FC12 footprint areas are in excess as compared to that of SWNT, leading to broadened chirality selection of SWNTs. Moreover, if consideration is given to dynamic equilibrium of flavin surfactants between solution and on SWNT, increasing flavin concentration in would promote slightly overpopulated flavin on SWNT. As a consequence, crowded flavins on SWNT might further induce smaller d_t SWNT enrichment as evident by PLE maps from 1:4:8 protocol. It is noteworthy that this scenario is only applicable to highly iSWNT dispersion and preferential interaction of flavin with SWNT rather than flavin self association in solution.

Next, a trend was seen in Γ of PL bands. The e_{22}^S and e_{11}^S bands of flavin-SWNT dispersed in various solvents were successfully analyzed through deconvolution of excitation and emission spectra of PLE maps by using Lorentzian fitting. Lorentzian fitting successfully simulated the overall excitation and emission spectra from various dispersions derived from different solvents (Figs. S5A–G for benzene to water dispersions, see SI for detailed explanation for the validity of fitting), and e_{22}^S , e_{11}^S , and Γ 's of each chirality from various solvents were obtained (Table S2). In Fig. S6 is shown the representative Γ variation in the (8,6) PL peak. Initially, Γ of (8,6) progressively increases from *ca.* 20 meV–42 meV in proceeding from benzene to water. This result suggests that heterogeneous broadening of (8,6) occurs, indicating that deviation takes place from ideal helical wrapping of the isoalloxazine ring. This is presumably a consequence of partial disruption of the H-bonded helical structure of isoalloxazine (Fig. 1B) owing to the H-bonding capability of solvents (i.e., ethyl acetate, THF, acetone, and water). It is noteworthy that comparison of absorption spectra and PLE maps shows that Stark shift of e_{11}^S (i.e., (8,6)) is quite small (from 2 to 4.5 meV). This value is in agreement with the one previously reported for semiconducting SWNT [50].

The above observations demonstrate that FC12-SWNT dispersions have PL activities in various organic solvents (i.e., *p*-xylene, benzene, toluene, ethyl acetate, THF, and acetone) [12]. It is noteworthy that, unlike other dispersions, SWNT dispersions from

solvents having medium ϵ values (i.e., ethyl acetate and acetone) were obtained only by using lower centrifugal force (i.e., 4 kg) because those derived from the higher centrifugal force 20 kg precipitate presumably caused by forming SWNT bundles. This result suggests that surfactant-SWNT nanoconjugates in medium ϵ solvents, in which FC12 has larger solubilities [12] (Table S1), have counterintuitively lower dispersibility than those formed in low ϵ solvents. FC12-SWNT dispersions do form in solvents which have higher solubilities (i.e., chloroform, methylenechloride, pyridine and methanol) but they do not display PL emission. This observation suggests that solvents in which FC12 has limited solubility (i.e., ca. 0.31 mg/mL FC12 in aromatic solvents) promote formation of iSWNTs that have profound PL activity.

In order to understand the contributions arising from background absorption, AFM height topographies from each dispersion were obtained. For this purpose, dispersed samples were dropcast onto a cleaned 285 nm thick SiO₂/Si substrate and the resulting samples were carefully washed with respective dispersing solvent to minimize possible solvent-driven bundling. Fig. 3A–G and Fig. S7 show respective height and phase images containing iSWNT, bSWNT, and CI, respectively, and Figs. S8A–G display additional AFM height images. Interestingly, relative contributions from each component are drastically different in each solvent. Specifically, i)

lower ϵ aromatic solvents (top row of Fig. 3) are highly populated with iSWNT, and higher ϵ polar solvents are populated with bSWNT, and ii) higher ϵ solvents contains lesser amounts of CI. The height limit of flavin-wrapped iSWNT was set to 3.0 nm considering an average d_t and distribution of HiPco (i.e., 1.0 nm \pm 0.3 nm), and summation of van der Waals (vdW) distances (two isoalloxazine layers + two layers of dodecyl side chain + vdW distance of AFM tip: 0.34 nm \times 5), as evident by representative AFM height and phase images (Figs. S9A and B, respectively) [32]. Benzene dispersion (Fig. 3A) contains a mixture of iSWNT and bSWNT, along with CI. Dispersions from *p*-xylene and toluene (Fig. 3B and C) contain mainly iSWNT and CI, which is in accordance with the sharp absorption of SWNT and relatively small background in absorption measurement. Interestingly, ethyl acetate dispersion (Fig. 3D) contains CI exclusively, suggesting background absorption originates from CI. THF and acetone dispersions contain mainly bSWNT having a height above 10 nm, and a lesser amount of CI. Water dispersion contains mainly bSWNT and iSWNT. Overall, dispersions in polar solvents such as THF, acetone, and water have the lowest CI contents. Offset height profiles with 3.0 nm FC12-iSWNT limit in gray (Fig. 3H) clearly displays these trends. These results suggest that dispersions in each solvent contain three different populations of iSWNT, bSWNT, and CI, and that those in polar higher ϵ solvents

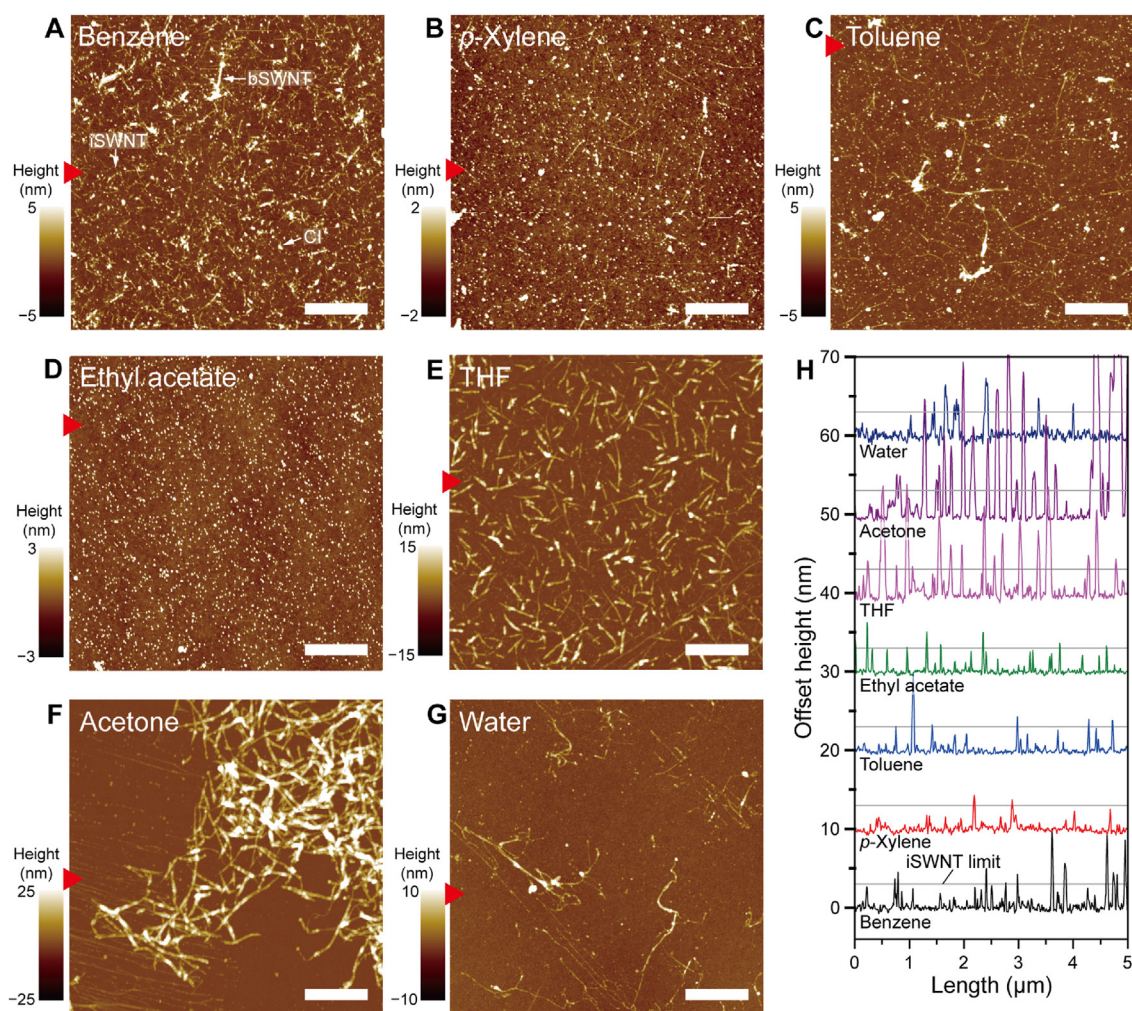


Fig. 3. (A to G) AFM height images of dispersions in each solvent. Scan sizes throughout the images were 5 $\mu\text{m} \times 5 \mu\text{m}$ with 512 \times 512 pixels. Scale bar: 1 μm . Triangles denote height profile positions for offset height profiles. (H) Offset height profiles from each solvent by 10 nm. Gray lines were drawn to indicate height limit of a iSWNT wrapped by flavin. (A colour version of this figure can be viewed online.)

and aromatic lower ϵ solvents are mainly populated by bSWNT and CI, respectively, on top of iSWNT. More quantitative evaluation of CI contents present in FC12-SWNT dispersion will be published elsewhere [51].

Since we have established the origin of the background contributions as non-radiating nanocarbon species such as bSWNT and CI, we were able to obtain Φ_R for various solvents by using equation (1) [12,52],

$$\Phi_R = \Phi_{ref} \times \frac{I_s \times \alpha_{ref} \times n_s^2}{I_{ref} \times \alpha_s \times n_{ref}^2} \quad (1)$$

where I is the integrated area of photoluminescence emission, α is the extinction coefficient at the excitation wavelength, and n is the refractive index of the solvent for the sample (s) and reference (ref), respectively. The extinction coefficient α was obtained from the respective peak height of the absorption band at the excitation wavelength, as described in Fig. 4A. Here, we focused on (7,6) chirality whose $e^{S_{22}}$ and $e^{S_{11}}$ bands are positions near 664 nm and 1150 nm, respectively. The concentration of all samples was adjusted to below 0.05 absorbance at 660 nm (Fig. S2). For the Φ_R calculations, background absorption denoted by β was discarded for the PL contribution, and only α was considered. Moreover, $e^{S_{11}}$ emission spectra obtained by excitation at 660 nm contain PL peaks originating from various sources (i.e., $e^{S_{22}}$ to $e^{S_{11}}$ emission ($e^{S_{22}}$ - $e^{S_{11}}$), electron-phonon interactions (e -ph) [53], and energy transfer from one to another SWNT [54,55]). Since they are associated with α , the PL areas were included to obtain (7,6) contributions from other components (Fig. 4B), assuming that absorbance and PL intensity of SWNT is proportional regardless of SWNT chiralities. The fraction of the PL from (7,6) over the sum of PL areas is considered to be absorbance fraction of (7,6) in α denoted as $\alpha_{(7,6)}$. The PL area of (7,6) divided by $\alpha_{(7,6)}$ results in Φ_R for $n = 1$ or $n = n_s$, calculated by using eqn (1) and given in Table S3. A similar treatment for other solvents gives the results shown in Figs. S10A–F. The calculated Φ_R normalized against that of benzene (i.e., $n = 1$) is depicted in Fig. 4C, which simulates a uniform flavin coating on SWNT. Clearly, aromatic solvents have greater Φ_R than other solvents (toluene, p -xylene, and benzene in that order). Similar pattern is also seen when $n = n_s$ where n_s is a refractive index of solvent. Overall, the Φ_R difference between solvents is in excess of 10 times. Highest and lowest Φ_R are obtained with toluene and ethyl acetate dispersions, respectively. These results are in line with SWNT bundling tendencies observed in the aforementioned AFM studies. Although α is thought to be from iSWNT, bSWNT also partially contributes to α and a subsequent Φ_R reduction, which is the case of polar higher ϵ solvents.

2.2. Role played by side chain δ in governing properties of flavin-SWNT dispersions

The specific chirality and smaller d_t enrichment of flavin-SWNT produced using respective low and high flavin concentrations are a consequence of interactions with solvents and are related to the properties of the interfacing surfactant and, in particular those imparted by the N -linked side chains. To gain information about this issue, we evaluated the solvent miscibilities of dodecyl and d -ribityl phosphate, which are the respective side chains present in FC12 and FMN. Minimization of the enthalpy of mixing (H_{mix}) between the solvent and side chain results in high purity dispersion by compensating the negative entropy factor in the Gibbs energy. H_{mix} for a binary system is given by $H_{mixing} = \phi_1 \phi_2 (\delta_1 - \delta_2)^{1/2}$, where ϕ_n and δ_n are the mole fractions and δ of each component, respectively. This relationship suggests that minimization of differences in δ leads to lower H_{mix} . The δ values were calculated using van Krevelen methods formulation given by equation (2) [56],

$$\delta = \sqrt{\delta_D^2 + \delta_P^2 + \delta_H^2} \quad (2)$$

where δ_D , δ_P , and δ_H are the molar attraction due to molar dispersion forces, molar polarization forces, and H-bonding, respectively. A further contribution to the δ values stems from molar volume and energy (or force) according to eqn (3),

$$\delta_D = \frac{\Sigma F_D}{V_i}, \quad \delta_P = \frac{\sqrt{\Sigma F_P^2}}{V_i}, \quad \delta_H = \frac{\sqrt{\Sigma E_H}}{V_i} \quad (3)$$

where F_D is the molar attraction constant due to molar dispersion forces, F_P^2 is the molar attraction constant due to molar polarization forces, E_H is the H-bonding energy and V_i is the group contribution to molar volume.

In Fig. 5A are listed δ_D , δ_P and δ_H contributions associated with solvents, the dodecyl group of FC12, and the d -ribityl phosphate group of FMN (see dashed circles). The respective δ_D , δ_P and δ_H values for the flavin sidechains, calculated using eqn (3), are 16.1, 0 and 0 for the dodecyl side chain, and 20.2, 19.6 and 26.2, for the d -ribityl phosphate side chain (see Supplementary note in SI). These values along with those from various solvents are displayed in Table S1. In general, the smaller δ difference ($\Delta\delta$) below 5 MPa^{1/2} indicates good miscibility of two components. The $\Delta\delta$ s of benzene, p -xylene, and toluene against dodecyl side chains are 2.6, 1.9 and 2.2, respectively (Fig. 5C). Benzene showed the largest $\Delta\delta$ among three aromatic solvents. Those difference create a larger mixing enthalpy which causes the side chains to have a collapsed configuration which in turn might broaden chirality selection by obscuring binding-affinity based selection. $\Delta\delta$ s of other solvents

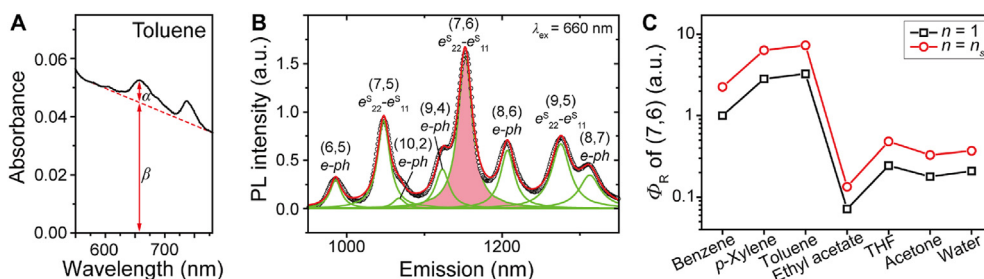


Fig. 4. Measurements of Φ_R of (7,6) of a toluene dispersion. (A) Absorbance of a dilute solution and its analytical contribution from SWNT (α) and background (β) to obtain net absorbance. (B) PL emission spectra containing I_{PL} of (7,6). $e^{S_{22}}$ - $e^{S_{11}}$ and e -ph denote PL from $e^{S_{22}}$ to $e^{S_{11}}$ transitions and electron-phonon interaction, respectively. (C) Φ_R variations of (7,6) chirality over various solvents by using eqn. (1) for $n = 1$ (black) or $n = n_s$ (red). (A colour version of this figure can be viewed online.)

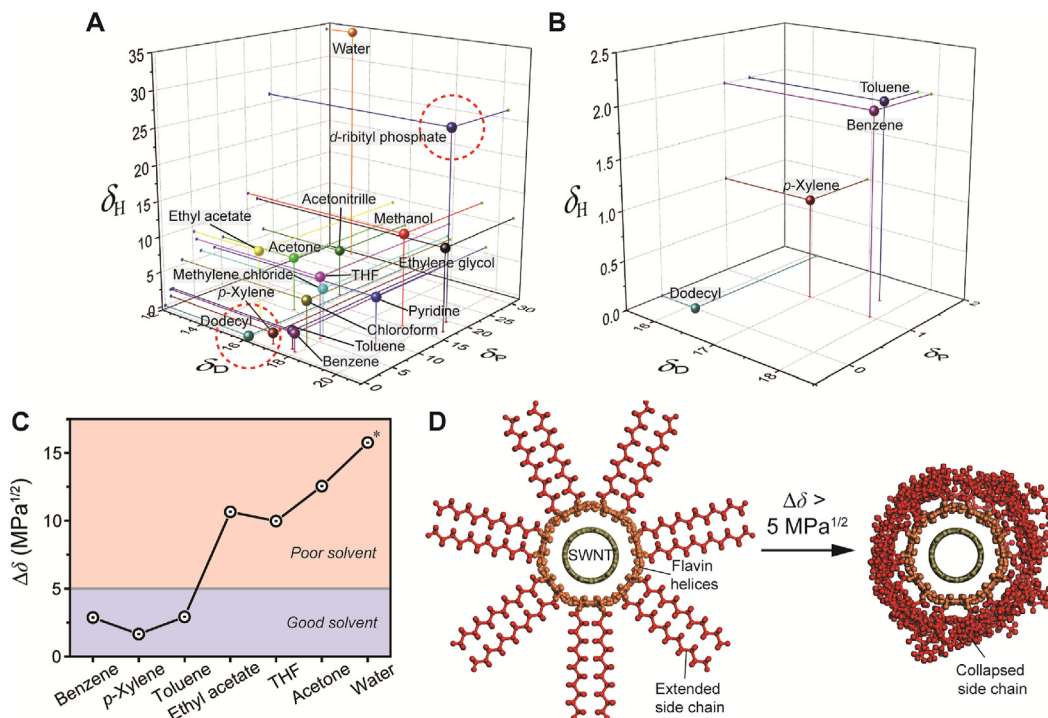


Fig. 5. (A) δ plot of dodecyl and *d*-ribityl phosphate side chains highlighted in red dash circles, along with those of various solvents denoted by spheres. Red, blue, and green dots indicate drop line for each plane. (B) Zoom-in of the region dodecyl side chain against aromatic solvents in the δ plot. (C) Solvent vs. $\Delta\delta$ plot against dodecyl side chain. Asterisk denotes $\Delta\delta$ obtained *d*-ribityl phosphate against water. Pictorial illustration of the (D) extended (left) vs. collapsed (right) side chains of isoalloxazine helical assembly on an SWNT driven by $\Delta\delta$. Gray, orange, and red colors denote SWNT, isoalloxazine, and dodecyl side chains, respectively. (A colour version of this figure can be viewed online.)

against dodecyl side chain display much large values (i.e., acetone: 12.6, THF: 10.0, and ethyl acetate: 10.7). Likewise, $\Delta\delta$ of water against *d*-ribityl phosphate group is 15.8. These results are in correspondence with the experimental findings that aromatic solvents are strongly associated with dodecyl side chain and promote formation of high purity FC12-SWNT dispersions that have narrow absorption and PL emission bands [12]. Likewise, ethyl acetate and THF whose δ are farther from that of the dodecyl side chain lead to moderate FC12-SWNT dispersions that have low PL emission with moderate I . In addition, it is not a coincidence that aromatic solvents have larger SWNT dispersibility, as evidenced by absorbances in Fig. S2, owing to closest match of δ between dodecyl side chain and solvents.

Special attention needs to be given to $\Delta\delta$ s of aromatic solvents to understand the role they play in creating SWNT dispersions (Fig. 5B). Toluene and *p*-xylene dispersions, which show large e_{22}^S to e_{11}^S extinction coefficients over background and higher Φ_R , display the lowest $\Delta\delta$ s. Especially, toluene and *p*-xylene dispersions display certain chirality selections with lower flavin concentrations. A closer match of δ to that of the dodecyl side chain as well as a lower flavin concentration enables this chirality discrimination. It is noteworthy that although benzene, *p*-xylene and toluene have $\Delta\delta < 5 \text{ MPa}^{1/2}$, the isoalloxazine contribution on the SWNT surface was not included in the δ calculation owing to the fact that it adopts a half exposed configuration (Fig. 5D). The inclusion of isoalloxazine ring would have resulted in a higher $\Delta\delta$ owing to mainly $\Delta\delta_H$. In fact, the solvatochromic parameter is further categorized using H-bond donor and acceptor values of various solvents [57]. Especially, while their H-bond donor values are zero, toluene, benzene and *p*-xylene have respective H-bonding acceptor values of 0.11, 0.10 and 0. The H-bonding acceptor ability might enhance solvation of the isoalloxazine moiety on SWNT by toluene which has the highest Φ_R . The slight departure of selectivity observed for benzene dispersion

seems to result from H-bonding interaction between the flavin moiety and benzene in addition to the aforementioned $\Delta\delta$. This scenario is pictorially portrayed in Fig. 5D. A $\Delta\delta$ below $5 \text{ MPa}^{1/2}$ prompts the side chain of FC12 to adopt an extended configuration whereas a larger $\Delta\delta$ results in a collapsed side chain owing to a larger H_{mix} . Furthermore, the collapsed and consequently tightened flavin-SWNT structure favors smaller d_t SWNT selectivity which takes place in higher ϵ solvents. In addition, the collapsed side chain would facilitate production of the bSWNT structure by allowing the presence of other SWNTs in vicinity. For example, the dodecyl side chain in FC12-SWNT in toluene and *p*-xylene exists in an extended conformation which facilitates generation of highly individualized SWNT dispersions, with high stability and PL intensity [12]. As the ϵ value of the solvent increases, large $\Delta\delta$ leads to production of a collapsed side chain conformation in conjunction with an increased formation of bSWNT structures.

2.3. Solvatochromism of flavin-SWNTs dispersions

One of the most important questions addressed in this effort is whether intimate contact between the flavin isoalloxazine ring and the SWNT sidewalls affect solvatochromism of the dispersions. Since e_{11}^S and e_{22}^S of SWNT are governed by longitudinal polarizability [58], they are likely impacted by interactions with transition dipoles of flavin that are oriented nearly parallel to longitudinal axis [59]. A molecular simulation of lumiflavin in various solvents was performed by using density functional theory (DFT) to gain insight into the electronic effects of surfactant wrapping (see Methods). In Table S4 are displayed isoelectric contours and energies of highest occupied molecular orbitals (HOMO) and lowest unoccupied molecular orbitals (LUMO) of lumiflavin. The calculated isoelectric contours are in excellent agreement with those determined recently [60]. The increase in solvent ϵ value brought about

by changing from *p*-xylene to water results in a minute narrowing (1 meV) of the HOMO/LUMO energy gap (Figs. S11A and B). This finding is in line with UV–vis absorption spectra of FC12 and FMN (Fig. S12) in various solvents where the position of the lowest wavelength vibronic band does not change significantly (*i.e.*, in between 443 and 447 nm). In addition, DFT calculations indicate that the difference between the *d*-ribityl phosphate and *n*-dodecyl side chains would weakly affect the electronic structure of the isoalloxazine ring. These results indicate that helical wrapping of an isoalloxazine in various solvents provides minimal electronic perturbation on SWNT.

We next addressed the issue of whether the isoalloxazine can directly influence e_{ii}^S of SWNT. Solvatochromic shifts (Δe_{ii}^S) of the FC12/HiPco/benzene system, which corresponds to e_{ii}^S for SWNTs in vacuum ($e_{ii}^{S, vac}$) minus those for FC12/HiPco/benzene ($e_{ii}^{S, solvent}$), are displayed in Fig. 6 as a function of the d_t of the SWNT. Red and black symbols correspond to FC12-derived Δe_{22}^S and Δe_{11}^S according to d_t of SWNT chiralities, respectively, and green and blue symbols represent the respective SDS-derived Δe_{22}^S and Δe_{11}^S which were obtained from the literature [1,58]. Measured solvatochromic shifts are given relative to $e_{ii}^{S, vac}$, which was determined using the relationship in eqn (4) originally developed by others [1,58].

$$e_{ii}^{S, vac} = \frac{1241 \text{ eV}\cdot\text{nm}}{A_1 + A_2 d_t} + A_3 \frac{\cos(3\theta)}{d_t^2} \quad (4)$$

where θ is chiral angle of SWNT [61], and A_1 , A_2 and A_3 are parameters determined from the published values for $e_{ii}^{S, vac}$ (see SI for detailed explanation) [58]. When both trends are fitted using linear regressions, Δe_{22}^S and Δe_{11}^S of the FC12/benzene system have overall negative slopes (*i.e.*, -0.29 and -0.14 eV/nm) and a large offset with respect to $e_{ii}^{S, vac}$. The observation that these values are much larger than Δe_{ii}^S trends seen for SWNT wrapped by SDS [58] (*i.e.*, Δe_{22}^S and Δe_{11}^S : 0.23 and -0.12 eV/nm), shows that SWNTs with smaller d_t display larger solvatochromic shifts. The offset energy difference in Δe_{ii}^S as compared to those from SDS likely originates from photoinduced charge transfer from the SWNT to the isoalloxazine ring [4]. Moreover, recent calculations [62] show that flavin coverage on varying SWNT does not change much, suggesting a minimal effect of surface flavin on SWNT [62].

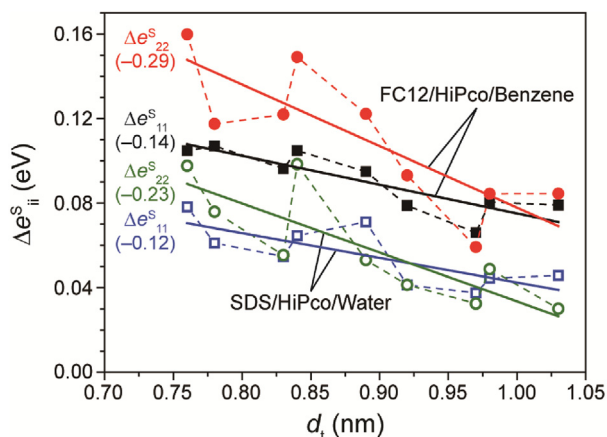


Fig. 6. Δe_{ii}^S trends as a function of SWNT d_t against $e_{ii}^{S, vac}$. Dashed lines given for visual aid. Solid lines are obtained from linear regression analysis from flavin/SWNT/solvent systems and SDS/SWNT/water systems for comparison. Numbers in brackets denote slopes of linear fits of eV/nm. (A colour version of this figure can be viewed online.)

Solvatochromism of the SWNTs within the isoalloxazine system was investigated next. Inspection of the plot given in Fig. 7A clearly demonstrates that with increasing ϵ of the solvent, e_{11}^S and e_{22}^S undergo shifts that are dependent on the SWNT family (*i.e.*, $Fam = 2n + m$) [61], and d_t . The SWNT family has a branch-like structure stemming from near armchair SWNT (gray dashed line), and as ϵ increases the cross-points of e_{11}^S and e_{22}^S display rough bathochromic shifts except in the case of (8,3) and (8,7) chiralities. In addition, the solvent induced optical shifts are d_t dependent. For example, (8,6), (8,7) and (6,5) show the lowest spreads in cross-points of e_{11}^S and e_{22}^S occurred by varying solvents (*i.e.*, (8,6): 9.2 meV and 8.8 meV, (8,7): 9.3 meV and 5.8 meV, (6,5): 10.3 meV and 13.9 meV, respectively. See Table S2). In contrast, (7,6) displays the largest spreads in e_{11}^S and e_{22}^S (*i.e.*, 25.5 meV and 23.9 meV, respectively). This seems to originate from binding affinity difference between flavin and various SWNT chiralities in which tight wrapping of flavin is less amenable to solvent-induced PL changes. An earlier comparison of the relative binding affinities of FMN against other surfactant sodium dodecyl benzene sulfate on SWNTs showed that (8,6) and (8,7) has the strongest binding affinity caused by π - π interaction with the isoalloxazine self-assembly owing to the d_t -matching 8₁ helix [62] whereas other smaller d_t chiralities adapt 7₁ or 7.5₁ helices [62]. Furthermore, (8,6) and (8,7) chiralities exhibit a quasi-epitaxial arrangement between 8₁ flavin helix and underlying SWNT, whereas (7,6) chirality is wrapped by 7.5₁ flavin helix and show less commensurability [32,62,63]. Therefore, the incommensurability of (7,6) chirality with the isoalloxazine assembly might be a contributor to the larger bathochromic shift. Trends of this type are observed in the Δe_{22}^S and Δe_{11}^S with respect to those of benzene vs. ϵ shown in Fig. 7B to C. Clearly, most of slopes in these plots are negative, indicating bathochromic shifts in e_{11}^S and e_{22}^S . However, e_{11}^S of (8,7) and e_{22}^S of (9,4) show slight hypsochromic shifts for a currently unexplainable reason. Especially, when Fig. 7B is compared to solvatochromism observed in microencapsulation of solvents in SDS-SWNT (Fig. S13), a smaller standard deviation and less solvatochromic spread occurs as ϵ increases. These results are in stark contrast with those obtained using bare SWNTs where e_{11}^S and e_{22}^S exhibit larger bathochromic shift by 33–49 meV and 26–30 meV, with a tendency showing saturation at $\epsilon = 5$ without a significant (n, m) dependence. [23] The findings, which are in accord with the aforementioned results of DFT calculations, suggest that the isoalloxazine assembly serves as a solvatochromic protective layer that mitigates changes in optical transitions when ϵ varied.

3. Conclusion

In the investigation described above, we explored solvent-specific dispersion formation, relative quantum yield, and optical transition changes of SWNT controlled by amounts of flavin surfactants. The advent of flavin derivatives, which exfoliate SWNT individually in multiple solvents *via* precise helical wrapping motifs, has made an investigation of this type possible. Initial screening results suggests that solvents having larger solubilities for surfactants do not promote formation of SWNT dispersions whereas solvents having small and intermediate solubilities have respective good and poor abilities to form dispersion that have PL activities. For the dispersions having PL activities, selection of specific chirality in nanoconjugate formation between SWNTs and flavin derivatives is controlled by the size of the flavin footprint over SWNT surface area, in which flavin concentrations less than the those of the SWNT surface area lead to higher selectivity of specific chiralities. This phenomenon originates from binding

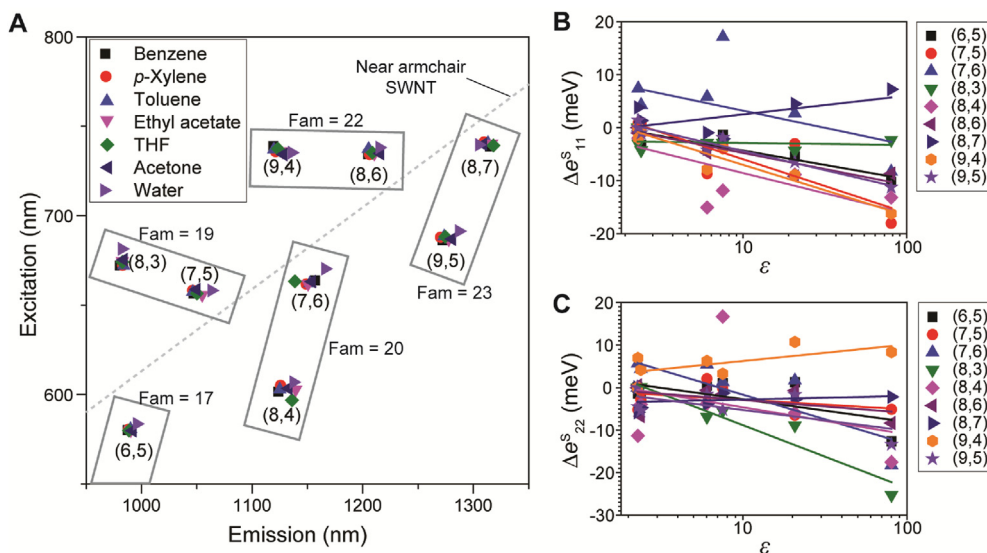


Fig. 7. Solvatochromism of SWNTs wrapped by flavins. (A) Deconvoluted e^S_{11} and e^S_{22} trends of SWNT dispersed in various solvents. Boxes indicate SWNT families. (B) Δe^S_{11} vs. ϵ and (C) Δe^S_{22} vs. ϵ plots of several SWNT chiralities in various solvents with respect to benzene. Solid lines originate from linear fits of the data. (A colour version of this figure can be viewed online.)

affinity, and higher flavin concentration results in broadened chirality distribution towards smaller diameter SWNT. Absorption spectra of SWNTs in aromatic lower ϵ solvents display sharp optical transitions and small background absorption whereas in polar higher ϵ solvents broadened optical transitions and larger background are observed. The origin of background absorptions according to solvents were investigated by using AFM measurements, the results of which show that aromatic solvents facilitate production of individualized SWNT and carbonaceous impurities, whereas polar higher ϵ solvents promote formation of bundled SWNT with lesser carbonaceous impurities. Understanding absorption contributions allows us to analyze the relative quantum yields in various solvents, and to show that aromatic solvents such as toluene and *p*-xylene give the highest PL. The PL, absorption and AFM trends are in line with solubility parameter δ for solvent-interacting with the flavin side chain. We speculate that δ difference controls whether the dodecyl side chain in FC12 exists in an extended or collapsed conformation owing to mixing enthalpy. Lastly, we observed solvatochromism of optical transition energies of SWNTs and showed that the solvent-dependent optical transitions have specific d_t dependences and family behavior of SWNT in that order. Departure of optical transitions from bare SWNT seems to originate from charge transfer between flavin and SWNT. Comparison within flavin assemblies shows that, in addition to the minute solvatochromism of isoalloxazine rings, isoalloxazine wrapping shields SWNTs from the environmental dielectric effect. SWNT chiralities that have higher binding affinities with flavins display the smallest bathochromic shifts whereas intermediate d_t SWNTs exhibit larger solvent dependent changes presumably owing to incommensurability between flavin helix and SWNT chirality pattern. The solvent-specific enrichment of SWNT chirality is especially useful for the purpose of selecting specific SWNT chiralities by combining a choice of solvent and SWNTs with different diameter distributions (i.e., CoMoCAT [64], HiPco [65], and PSWNT [5]). Solvent-specific quantum yields of SWNTs are useful for designing novel PL-based sensory and Near IR imaging system. The rational design of side chain by taking into consideration solubility parameters will serve as a strategy to produce hierarchical SWNT morphologies for various optoelectronic applications.

4. Methods

4.1. Materials and instrumentation

All solvents were reagent grade and were used without further purification unless otherwise mentioned. FC12 was synthesized using a previously described procedure [5,12]. The mono-sodium salt form of FMN with a purity greater than 93% was purchased from TCI (Tokyo, Japan). All solvents were dried over molecular sieves (3 Å pore size, 1–2 mm beads, Alfa Aesar) for a day prior to dispersion of SWNT. SWNTs prepared by using HiPco [65] were purchased from NanoIntegris Inc. (Raw grade, batch #: HR29-073, Canada, minimum SWNT contents >65%) and have a median d_t with distributions of 1.0 ± 0.3 nm. All measurements were performed at 20 °C unless otherwise noted. UV–vis–NIR absorption with wavelength extension kit up to 3200 nm were recorded on a spectrophotometer (V-770, JASCO, Japan) with absorption cuvettes having 10 mm (Lot. No.: 100-10-40, QS, Hellma Analytics, Germany) or 1 mm path length (21/Q/1, Starna scientific, UK) unless otherwise noted. Absorbances were measured via double beam configuration. UV–vis regions are dispersed by 1200 lines/mm grating and NIR region is dispersed by 300 lines/mm grating. D₂ lamp and Tungsten–Iodine lamps were used for excitations for 190–350 nm and 330 nm–3200 nm, respectively. Wavelength accuracy was 0.3 nm for UV–vis and 1.5 nm for NIR regions, respectively. Photometric accuracy is 0.0015 for 0 to 0.5 abs, and 0.0025 abs for 0.5 to 1 abs. Detectors for UV–vis and NIR regions were photomultiplier tube (PMT) and PbS photoconductive cell. The dispersions were diluted so that e^S_{22} are below 0.05 to minimize reabsorption [66]. AFM measurement was conducted by using a commercially available AFM (NX10, Park systems, Republic of Korea). An Al-coated silicon cantilever with a spring constant 37 N/m, a resonance frequency of 300 kHz, and quoted radius of ca. 6 nm (ACTA, App Nano, CA, USA) were utilized to measure height topographies. Typically, a 512×512 pixel image was collected from $5 \mu\text{m} \times 5 \mu\text{m}$ size area. Prior to AFM measurements, 200 μL of the PSWNT dispersion was dropcasted on 285 nm-thick SiO₂/Si substrates and dried for 10 min. Then, the substrate was rinsed with a dispersing solvent several times until no green fluorescence

originating from flavin derivatives was observed by using a hand-held UV lamp (i.e., 365 nm). The rinsed substrate was dried by N₂ blowing. The measured height and phase topographies were analyzed by XEI 4.3.4 program (Park systems, Republic of Korea). For pictorial illustration of flavin-wrapped (8,6) SWNT, their atomic coordinates were obtained from the literature [32], and VMD software was used for molecular visualization [67].

4.2. Dispersion of SWNTs using FC12 or FMN

Dispersions of 1 mg of HiPco (1 mg, 83 μ mol in carbon equiv), and 4 mg (9.7 μ mol) of FC12 (or FMN) in 4 mL of dried solvents were prepared by initial 15 min bath-sonication (Branson 1510, 70 W, CT, USA), followed by tip sonication for 1 h at 300 W (13 mm tip, VCX750, 750 W, Sonics & Materials, CT, USA). The resulting dispersions were subjected to centrifugation at 20,000 g for 2 h with a fixed angle rotor (Avanti J-26 XPI and JA-25.50, respectively, Beckman Coulter, CA, USA) at the room temperature using organic solvent-tolerant centrifugation tubes (50 mL, Cat. #: 3114-0050, fluorinated poly(ethylene)-co-poly(propylene), Nalgene, NY, USA). Similar dispersions from ethyl acetate and acetone were further conducted with reduced centrifugation force (i.e., 4000 g) for 2 h to obtain iSWNT. The 80% supernatant was carefully collected. Similar sonication conditions using FMN produces poor dispersion, and consequently we opt to use 2 h at 300 W probe sonication, followed by higher centrifugation force at 30,000 g for 2 h. Likewise, the dispersions with 1:4:0.5, 1:4:0.75, 1:4:1, 1:4:8 protocols were prepared.

4.3. PLE measurements and analysis

Fluorescence measurements were conducted on a spectrofluorometer (Jobin-Yvon Spex Fluorolog 3–211, Horiba, Kyoto, Japan) equipped with Xe arc lamp (220–1000 nm, 450 W, ozone-free, Ushio, Japan), a subtractive double monochromator for excitation source and monochromator, respectively, and a spectrometer (150 gratings/mm, iHR320) with a LN-cooled InGaAs array detector (512 \times 1 pixels, Symphony_IGA_1700) for emission. The intensities were corrected for instrumental variations in excitation intensity and detection sensitivity. Slit widths of excitation and emission wavelengths are 14 nm and 10 nm, respectively. Excitation increase for the PLE mapping was 5 nm interval. 1 cm path length fluorescence cuvette (QS grade, Hellma) was utilized, and emission was collected from sample with 90° against excitation beam. The SWNT dispersions were diluted so that e_{22}^S are approximately below 0.05 to minimize readsorption [66]. All measurements were conducted at 20 °C. PL chirality assignments of semiconducting SWNTs were based on PL pattern matching of PLE map, reported by O'Connell et al. [2,32]. Respective integration times for dispersion samples varies from 3 s to 50 s. Those values are normalized to compare relative quantum yield. e_{11}^S and e_{22}^S of SWNT was analyzed by extracting from excitation and emission matrix data of PLE map. Initially, emission spectra at certain excitation were deconvoluted by Lorentzian fitting to obtain e_{11}^S . Similarly, excitation spectra near the determined e_{11}^S were deconvoluted.

4.4. Molecular simulation of lumiflavin

DFT calculations of lumiflavin were carried out using the Gaussian 09 package [68]. Prior to calculation, geometry optimization of lumiflavin in various solvents was carried out with the connectivity of N₁₀ in lumiflavin as tetrahedral configuration (Fig. 1A), according to previous work [32]. Geometry optimization and energy minimization were performed using hybrid functional

Becke-3-Lee-Yang-Parr (B3LYP) with a 6-31G⁺(d, p) basis set using polarized continuum model (PCM) with integral equation formalism (IEF) for solvents.

CRedit authorship contribution statement

In-Seung Choi: prepared samples and conducted measurements. **Minsuk Park:** prepared samples and conducted measurements. **Eunhye Koo:** prepared samples and conducted measurements. **Sang-Yong Ju:** conceived the idea and wrote the manuscript.

Declaration of competing interest

The authors declare that they have no known competing financial interests or personal relationships that could have appeared to influence the work reported in this paper.

Acknowledgement

This research was mainly supported by the Basic Science Research Program through the National Research Foundation of Korea (NRF) funded by the Ministry of Education, Science, and Technology (2020R1F1A1076983, 2020R1A4A1017737, and in part 2019R1A6A3A13091240). The computational calculation was supported by the Supercomputing Center/Korea Institute of Science and Technology Information (KISTI) with supercomputing resources including technical support. Prof. S. J. and Prof. G. L. gratefully acknowledge support from USyd-Yonsei Partnership Collaboration Awards.

Appendix A. Supplementary data

Supplementary data to this article can be found online at <https://doi.org/10.1016/j.carbon.2021.08.054>.

References

- [1] S.M. Bachilo, M.S. Strano, C. Kittrell, R.H. Hauge, R.E. Smalley, R.B. Weisman, Structure-assigned optical spectra of single-walled carbon nanotubes, *Science* 298 (5602) (2002) 2361–2366.
- [2] M.J. O'Connell, S.M. Bachilo, C.B. Huffman, V.C. Moore, M.S. Strano, E.H. Haroz, et al., Band gap fluorescence from individual single-walled carbon nanotubes, *Science* 297 (5581) (2002) 593–596.
- [3] E. Kymakis, G.A.J. Amaratunga, Single-wall carbon nanotube/conjugated polymer photovoltaic devices, *Appl. Phys. Lett.* 80 (1) (2002) 112–114.
- [4] M. Mollahosseini, E. Karunaratne, G.N. Gibson, J.A. Gascón, F. Papadimitrakopoulos, Fullerene-assisted photoinduced charge transfer of single-walled carbon nanotubes through a flavin helix, *J. Am. Chem. Soc.* 138 (18) (2016) 5904–5915.
- [5] M. Park, S. Kim, H. Kwon, S. Hong, S. Im, S.-Y. Ju, Selective dispersion of highly pure large-diameter semiconducting carbon nanotubes by a flavin for thin-film transistors, *ACS Appl. Mater. Interfaces* 8 (35) (2016) 23270–23280.
- [6] M. Zhao, Y. Chen, K. Wang, Z. Zhang, J.K. Streit, J.A. Fagan, et al., DNA-directed nanofabrication of high-performance carbon nanotube field-effect transistors, *Science* 368 (6493) (2020) 878–881.
- [7] M. Park, K.-I. Hong, S.-M. Jin, E. Lee, W.-D. Jang, S.-Y. Ju, Helical assembly of flavin mononucleotides on carbon nanotubes as multimodal near-IR Hg(II)-Selective probes, *ACS Appl. Mater. Interfaces* 11 (8) (2019) 8400–8411.
- [8] K. Welscher, Z. Liu, S.P. Sherlock, J.T. Robinson, Z. Chen, D. Daranciang, et al., A route to brightly fluorescent carbon nanotubes for near-infrared imaging in mice, *Nat. Nanotechnol.* 4 (11) (2009) 773–780.
- [9] Z. Liu, S. Tabakman, S. Sherlock, X. Li, Z. Chen, K. Jiang, et al., Multiplexed five-color molecular imaging of cancer cells and tumor tissues with carbon nanotube Raman tags in the near-infrared, *Nano Res* 3 (3) (2010) 222–233.
- [10] X. Yu, B. Munge, V. Patel, G. Jensen, A. Bhirde, J.D. Gong, et al., Carbon nanotube Amplification strategies for highly sensitive immunodetection of cancer biomarkers, *J. Am. Chem. Soc.* 128 (34) (2006) 11199–11205.
- [11] Z. Liu, M. Winters, M. Holodniy, H. Dai, siRNA delivery into human T cells and primary cells with carbon-nanotube transporters, *Angew. Chem. Int. Ed.* 46 (12) (2007) 2023–2027.
- [12] S.-Y. Ju, W.P. Kopcha, F. Papadimitrakopoulos, Brightly fluorescent single-walled carbon nanotubes via an oxygen-excluding surfactant organization,

- Science 323 (5919) (2009) 1319–1323.
- [13] A. Nish, J.-Y. Hwang, J. Doig, R.J. Nicholas, Highly selective dispersion of single-walled carbon nanotubes using aromatic polymers, *Nat. Nanotechnol.* 2 (10) (2007) 640–646.
 - [14] F. Chen, B. Wang, Y. Chen, L.-J. Li, Toward the extraction of single species of single-walled carbon nanotubes using fluorene-based polymers, *Nano Lett.* 7 (10) (2007) 3013–3017.
 - [15] F. Papadimitrakopoulos, S.-Y. Ju, Purity rolled up in a tube, *Nature* 450 (7169) (2007) 486–487.
 - [16] H.W. Lee, Y. Yoon, S. Park, J.H. Oh, S. Hong, L.S. Liyanage, et al., Selective dispersion of high purity semiconducting single-walled carbon nanotubes with regioregular poly(3-alkylthiophene)s, *Nat. Commun.* 2 (1) (2011) 541.
 - [17] A.V. Naumov, S. Ghosh, D.A. Tsybolski, S.M. Bachilo, R.B. Weisman, Analyzing absorption backgrounds in single-walled carbon nanotube spectra, *ACS Nano* 5 (3) (2011) 1639–1648.
 - [18] M.E. Itkis, D.E. Perea, S. Niyogi, S.M. Rickard, M.A. Hamon, H. Hu, et al., Purity evaluation of as-prepared single-walled carbon nanotube soot by use of solution-phase near-IR spectroscopy, *Nano Lett.* 3 (3) (2003) 309–314.
 - [19] M.E. Itkis, D.E. Perea, R. Jung, S. Niyogi, R.C. Haddon, Comparison of analytical techniques for purity evaluation of single-walled carbon nanotubes, *J. Am. Chem. Soc.* 127 (10) (2005) 3439–3448.
 - [20] J.-Y. Hwang, A. Nish, J. Doig, S. Douven, C.-W. Chen, L.-C. Chen, et al., Polymer structure and solvent effects on the selective dispersion of single-walled carbon nanotubes, *J. Am. Chem. Soc.* 130 (11) (2008) 3543–3553.
 - [21] A. Marini, A. Muñoz-Losa, A. Biancardi, B. Mennucci, What is Solvatochromism? *J. Phys. Chem. B* 114 (51) (2010) 17128–17135.
 - [22] S. Nigam, S. Ratan, Principles and applications of solvatochromism, *Appl. Spectrosc.* 55 (11) (2001), 362A–70A.
 - [23] Y. Ohno, S. Iwasaki, Y. Murakami, S. Kishimoto, S. Maruyama, T. Mizutani, Excitonic transition energies in single-walled carbon nanotubes: dependence on environmental dielectric constant, *Phys. Status Solidi B* 244 (11) (2007) 4002–4005.
 - [24] R.K. Wang, W.-C. Chen, D.K. Campos, K.J. Ziegler, Swelling the micelle core surrounding single-walled carbon nanotubes with water-immiscible organic solvents, *J. Am. Chem. Soc.* 130 (48) (2008) 16330–16337.
 - [25] C.A. Silvera-Batista, R.K. Wang, P. Weinberg, K.J. Ziegler, Solvatochromic shifts of single-walled carbon nanotubes in nonpolar microenvironments, *Phys. Chem. Chem. Phys.* 12 (26) (2010) 6990–6998.
 - [26] J.G. Duque, L. Oudjedi, J.J. Crochet, S. Tretiak, B. Lounis, S.K. Doorn, et al., Mechanism of electrolyte-induced brightening in single-wall carbon nanotubes, *J. Am. Chem. Soc.* 135 (9) (2013) 3379–3382.
 - [27] B.A. Larsen, P. Deria, J.M. Holt, I.N. Stanton, M.J. Heben, M.J. Therien, et al., Effect of solvent polarity and electrophilicity on quantum yields and solvatochromic shifts of single-walled carbon nanotube photoluminescence, *J. Am. Chem. Soc.* 134 (30) (2012) 12485–12491.
 - [28] J. Gao, W. Gomulya, M.A. Loi, Effect of medium dielectric constant on the physical properties of single-walled carbon nanotubes, *Chem. Phys.* 413 (2013) 35–38.
 - [29] N.R. Tummalala, A. Striolo, SDS surfactants on carbon nanotubes: aggregate morphology, *ACS Nano* 3 (3) (2009) 595–602.
 - [30] E.J. Wallace, M.S.P. Sansom, Carbon nanotube/detergent interactions via coarse-grained molecular dynamics, *Nano Lett.* 7 (7) (2007) 1923–1928.
 - [31] S.-Y. Ju, D.C. Abanulo, C.A. Badalucco, J.A. Gascón, F. Papadimitrakopoulos, Handedness enantioselection of carbon nanotubes using helical assemblies of flavin mononucleotide, *J. Am. Chem. Soc.* 134 (32) (2012) 13196–13199.
 - [32] S.-Y. Ju, J. Doll, I. Sharma, F. Papadimitrakopoulos, Selection of carbon nanotubes with specific chiralities using helical assemblies of flavin mononucleotide, *Nat. Nanotechnol.* 3 (6) (2008) 356–362.
 - [33] H. Oh, J. Sim, S.-Y. Ju, Binding affinities and thermodynamics of noncovalent functionalization of carbon nanotubes with surfactants, *Langmuir* 29 (35) (2013) 11154–11162.
 - [34] M. Park, J. Park, J. Lee, S.-Y. Ju, Scaling of binding affinities and cooperativities of surfactants on carbon nanotubes, *Carbon* 139 (2018) 427–436.
 - [35] S.-Y. Ju, F. Papadimitrakopoulos, Synthesis and redox behavior of flavin mononucleotide-functionalized single-walled carbon nanotubes, *J. Am. Chem. Soc.* 130 (2) (2008) 655–664.
 - [36] O.O. Ogunro, X.-Q. Wang, Quantum electronic stability in selective enrichment of carbon nanotubes, *Nano Lett.* 9 (3) (2009) 1034–1038.
 - [37] J. Sim, H. Oh, E. Koo, S.-Y. Ju, Effect of tight flavin mononucleotide wrapping and its binding affinity on carbon nanotube covalent reactivities, *Phys. Chem. Chem. Phys.* 15 (44) (2013) 19169–19179.
 - [38] K. Ozono, M. Fukuzawa, F. Toshimitsu, T. Shiraki, T. Fujigaya, N. Nakashima, Chiral selective chemical reaction of flavin-derivative-wrapped semiconducting single-walled carbon nanotubes based on a specific recognition, *Bull. Chem. Soc. Jpn.* 91 (11) (2018) 1646–1651.
 - [39] S. Kim, M. Jang, M. Park, N.-H. Park, S.-Y. Ju, A self-assembled flavin protective coating enhances the oxidative thermal stability of multi-walled carbon nanotubes, *Carbon* 117 (2017) 220–227.
 - [40] M. Park, S. Yoon, J. Park, N.-H. Park, S.-Y. Ju, Flavin mononucleotide-mediated formation of highly electrically conductive hierarchical monoclinic multi-walled carbon nanotube-polyamide 6 nanocomposites, *ACS Nano* 14 (2020) 10655–10665.
 - [41] W. Yoon, Y. Lee, H. Jang, M. Jang, J.S. Kim, H.S. Lee, et al., Graphene nanoribbons formed by a sonochemical graphene unzipping using flavin mononucleotide as a template, *Carbon* 81 (2015) 629–638.
 - [42] M. Ayán-Varela, J.I. Paredes, L. Guardia, S. Villar-Rodil, J.M. Munuera, M. Díaz-González, et al., Achieving extremely concentrated aqueous dispersions of graphene flakes and catalytically efficient graphene-metal nanoparticle hybrids with flavin mononucleotide as a high-performance stabilizer, *ACS Appl. Mater. Interfaces* 7 (19) (2015) 10293–10307.
 - [43] Z. Gao, C. Zhi, Y. Bando, D. Golberg, T. Serizawa, Noncovalent functionalization of disentangled boron nitride nanotubes with flavin mononucleotides for strong and stable visible-light emission in aqueous solution, *ACS Appl. Mater. Interfaces* 3 (3) (2011) 627–632.
 - [44] N. Nakashima, M. Fukuzawa, K. Nishimura, T. Fujigaya, Y. Kato, A. Staykov, Supramolecular chemistry-based one-pot high-efficiency separation of solubilizer-free pure semiconducting single-walled carbon nanotubes: molecular strategy and mechanism, *J. Am. Chem. Soc.* 142 (27) (2020) 11847–11856.
 - [45] J. Sim, S. Kim, M. Jang, M. Park, H. Oh, S.-Y. Ju, Determination of the absolute enantiomeric excess of the carbon nanotube ensemble by symmetry breaking using the optical titration method, *Langmuir* 33 (41) (2017) 11000–11009.
 - [46] M.S. Strano, C.B. Huffman, V.C. Moore, M.J. O'Connell, E.H. Haroz, J. Hubbard, et al., Reversible, band-gap-selective protonation of single-walled carbon nanotubes in solution, *J. Phys. Chem. B* 107 (29) (2003) 6979–6985.
 - [47] M.S. Strano, C.A. Dyke, M.L. Usrey, P.W. Barone, M.J. Allen, H. Shan, et al., Electronic structure control of single-walled carbon nanotube functionalization, *Science* 301 (5639) (2003) 1519.
 - [48] J. Zhang, Q. Chi, E. Wang, S. Dong, A comparative study on STM imaging and electrocatalytic activity of different surfaces modified with flavin adenine dinucleotide, *Electrochim. Acta* 40 (6) (1995) 733–744.
 - [49] E.J. Calvo, M.S. Rothacher, C. Bonazzola, I.R. Wheeldon, R.C. Salvarezza, M.E. Vela, et al., Biomimetics with a self-assembled monolayer of catalytically active tethered isalloxazine on Au, *Langmuir* 21 (17) (2005) 7907–7911.
 - [50] D. Song, F. Wang, G. Dukovic, M. Zheng, E.D. Semke, L.E. Brus, et al., Measurement of the optical Stark effect in semiconducting carbon nanotubes, *Appl. Phys. A* 96 (2) (2009) 283–287.
 - [51] Park M, Choi I-S, Ju S-Y. Carbonaceous impurity-excluded high-purity semiconducting carbon nanotube by controlled surfactant side chain length, to be submitted.
 - [52] J. Crochet, M. Clemens, T. Hertel, Quantum yield heterogeneities of aqueous single-wall carbon nanotube suspensions, *J. Am. Chem. Soc.* 129 (26) (2007) 8058–8059.
 - [53] M. Pföhl, D.D. Tune, A. Graf, J. Zaumseil, R. Krupke, B.S. Flavel, Fitting single-walled carbon nanotube optical spectra, *ACS Omega* 2 (3) (2017) 1163–1171.
 - [54] H. Qian, C. Georgi, N. Anderson, A.A. Green, M.C. Hersam, L. Novotny, et al., Exciton energy transfer in pairs of single-walled carbon nanotubes, *Nano Lett.* 8 (5) (2008) 1363–1367.
 - [55] D.Y. Joh, J. Kinder, L.H. Herman, S.-Y. Ju, M.A. Segal, J.N. Johnson, et al., Single-walled carbon nanotubes as excitonic optical wires, *Nat. Nanotechnol.* 6 (1) (2011) 51–56.
 - [56] D.W.V. Krevelen, *Properties of Polymers*, third ed., Elsevier, Press, Amsterdam, 1990. Amsterdam.
 - [57] M.J. Kamlet, J.L.M. Abboud, M.H. Abraham, R.W. Taft, Linear solvation energy relationships. 23. A comprehensive collection of the solvatochromic parameters, π^* , α , and β , and some methods for simplifying the generalized solvatochromic equation, *J. Org. Chem.* 48 (17) (1983) 2877–2887.
 - [58] J.H. Choi, M.S. Strano, Solvatochromism in single-walled carbon nanotubes, *Appl. Phys. Lett.* 90 (22) (2007) 223114.
 - [59] M. Sun, T.A. Moore, P.S. Song, Molecular luminescence studies of flavins. I. The excited states of flavins, *J. Am. Chem. Soc.* 94 (5) (1972) 1730–1740.
 - [60] L. Kammler, M. van Gastel, Electronic structure of the lowest triplet state of flavin mononucleotide, *J. Phys. Chem.* 116 (41) (2012) 10090–10098.
 - [61] M.S. Dresselhaus, G. Dresselhaus, P. Avouris, *Carbon Nanotubes: Synthesis, Structure, Properties and Applications*, Springer, Press, Berlin, 2001. Berlin.
 - [62] R. Sharifi, M. Samaraweera, J.A. Gascón, F. Papadimitrakopoulos, Thermodynamics of the quasi-epitaxial flavin assembly around various-chirality carbon nanotubes, *J. Am. Chem. Soc.* 136 (20) (2014) 7452–7463.
 - [63] O.V. Konevtsova, D.S. Roshal, V.P. Dmitriev, S.B. Rochal, Carbon nanotube sorting due to commensurate molecular wrapping, *Nanoscale* 12 (29) (2020) 15725–15735.
 - [64] Y. Maeda, M. Kanda, M. Hashimoto, T. Hasegawa, S. Kimura, Y. Lian, et al., Dispersion and separation of small-diameter single-walled carbon nanotubes, *J. Am. Chem. Soc.* 128 (37) (2006) 12239–12242.
 - [65] P. Nikolaev, M.J. Bronikowski, R.K. Bradley, F. Rohmund, D.T. Colbert, K.A. Smith, et al., Gas-phase catalytic growth of single-walled carbon nanotubes from carbon monoxide, *Chem. Phys. Lett.* 313 (1–2) (1999) 91–97.
 - [66] X. Wei, T. Tanaka, S. Li, M. Tsuzuki, G. Wang, Z. Yao, et al., Photoluminescence quantum yield of single-wall carbon nanotubes corrected for the photon reabsorption effect, *Nano Lett.* 20 (1) (2020) 410–417.
 - [67] W. Humphrey, A. Dalke, K. Schulten, Vmd - visual molecular dynamics, *J. Mol. Graph.* 14 (1996) 33–38.
 - [68] M.J. Frisch, G.W. Trucks, H.B. Schlegel, G.E. Scuseria, M.A. Robb, J.R. Cheeseman, et al., *Gaussian 09, Revision A.02*, Gaussian, Inc., Wallingford CT, 2009.

Dispersion of Carbon Nanotubes by Helical Flavin

Surfactants: Solvent Induced Stability and Chirality

Enrichment, and Solvatochromism

In-Seung Choi, Minsuk Park, Eunhye Koo, and Sang-Yong Ju^{,†}*

[†] Department of Chemistry, Yonsei University, Seoul 03722, Republic of Korea

* Correspondence E-mail: syju@yonsei.ac.kr

Table of Contents.....	S1
Detailed explanation of Lorentzian fitting.....	S2
δ calculations	S3
Full explanation of $e_{ii, vac}^S$	S4
Figure S1. pH-dependent absorption spectra changes of FMN-SWNT dispersion.....	S5
Figure S2. Absorption spectra changes according to different dispersion protocols and solvents.....	S6
Figure S3. Absorption spectra and PLE maps of flavin-SWNT from 1:4:0.5 and 1:4:0.75 protocols.....	S7
Figure S4. Metallic SWNT content change according to flavin concentration	S8
Figure S5. Lorentzian deconvolutions and PL positions determination of SWNT according to solvents	S9-S15
Figure S6. Γ change of (8,6) emission according to dispersion solvents	S16
Figure S7. The corresponding AFM phase images from Figure 3	S17
Figure S8. Additional AFM topographic images of SWNT dispersions from various solvents	S18
Figure S9. AFM height and phase images of representative individualized HiPco SWNT wrapped by FC12.....	S19
Figure S10. Absorbance and PL emission spectra measurements for Φ_R of (7,6) from each dispersion	S20
Figure S11. HOMO and LUMO levels of lumiflavin and energy gap depending on solvents	S21
Figure S12. Normalized absorption spectra changes of FC12 and FMN in various solvents	S21
Figure S13. Comparison of Figure 7B with micellarized microenvironments.....	S21
Table S1. ϵ , solubility, δ , and δ subcomponents of the used solvents in this study.....	S22
Table S2. SWNT chiralities and their deconvoluted e_{11}^S and e_{22}^S dispersed in various media.....	S23
Table S3. Φ_R calculations of (7,6) chirality according to solvent	S24
Table S4. Isoelectric contours of LUMO and HOMO and respective energy levels of lumiflavin	S25
Cited references	S26

Detailed explanation of Lorentzian fitting:

PLE map contains two-dimensional spreadsheet in which x and y axis denote emission and excitation in wavelength and their crosspoint indicates PL intensity. Initially, rough $e^{S_{11}}$ and $e^{S_{22}}$ positions are recoded for each (n, m) chiralities. For emission spectra for determination of $e^{S_{11}}$, nearest excitation wavelength was chosen, and the resulting emission spectrum was obtained from the matrix. The spectra were deconvoluted by Lorentzian shape for several reasons throughout the experiment although broadened PLE map is not well deconvoluted by the shape. Lorentzian shape well explains resonance behavior when excitation wavelength matches with electronic levels of materials. Gaussian fitting is better suited for broadening originating from heterogeneity including material size distribution. Voigt model which is combination of Lorentzian and gaussian fittings can explain both. However, voigt model has contribution from the combination of Lorentzian and gaussian, leading to uncertainty in FWHM owing to each fitting contribution. Therefore, we opted to use Lorentzian shape. Recent literature and references therein explains historical background for PL spectra fitting of SWNT.^{S1} Likewise, excitation spectrum for determination of $e^{S_{22}}$ was determined. It is noteworthy that resolution of excitation spectra is about 5 nm, providing less peak accuracy than that from $e^{S_{11}}$.

δ calculations:

δ were calculated from the contribution of δ_D , δ_P , δ_H using eqn 2 and 3. F_D , F_P , E_H and V were obtained from the reference S2. For the dodecyl side chain that contains 11 methylene and 1 methyl groups:

$$\delta_D = \Sigma F_D / V = (2970 + 420) / (177.1 + 33.5) = 3390 / 210.6 = 16.1$$

$$\delta_P = \text{sqrt}(\Sigma F_P^2) / V = 0$$

$$\delta_H = \text{sqrt}(\Sigma E_H / V) = 0$$

$$\delta = \sqrt{\delta_D^2 + \delta_P^2 + \delta_H^2} = 16.1$$

For the *d*-ribityl phosphate group that contains three hydroxyl, two methylene, three methine, and one PO₄ groups:

$$\delta_D = \Sigma F_D / V = (210 \times 3 + 270 \times 2 + 80 \times 3 + 740) / (10.0 \times 3 + 16.1 \times 2 - 1.0 \times 3 + 47) = 2150 / 106.2 = 20.2$$

$$\delta_P = \text{sqrt}(\Sigma F_P^2) / V = \text{sqrt}((500)^2 \times 3 + (1890)^2) / (10.0 \times 3 + 16.1 \times 2 - 1.0 \times 3 + 47) = 2079 / 106.2 = 19.6$$

$$\delta_H = \text{sqrt}(\Sigma E_H / V) = \text{sqrt}((20000 \times 3 + 13000) / (10.0 \times 3 + 16.1 \times 2 - 1.0 \times 3 + 47)) = \text{sqrt}(687.4) = 26.2$$

$$\delta = \sqrt{\delta_D^2 + \delta_P^2 + \delta_H^2} = 38.5$$

Full explanation of $e^{S_{ii}, \text{vac}}$:

$$e_{ii,vac}^S = \frac{1241 \text{ eV} \cdot \text{nm}}{A_1 + A_2 d_t} + A_3 \frac{\cos(3\theta)}{d_t^2}$$

The A_1 , A_2 , and A_3 parameters were fit by using the method of Choi and Strano^{S3} along with SWCNT $e^{S_{ii}}$ data from studies with dielectric environments similar to vacuum ($\epsilon \sim 1$). To calculate $e^{S_{11}}$ energies in eV, the parameters A_1 and A_2 are 61.1 nm and 1113.6 for $e^{S_{11}}$ and 87.4 nm and 613.7 for $e^{S_{22}}$, respectively. The value of A_3 depends on the SWNT (n, m) chirality. For $j = \text{mod}[(n - m), 3]$, A_3 is -0.077 and 0.143 eV·nm² for $e^{S_{11}}$ and $e^{S_{22}}$, respectively, if $j = 1$; A_3 is 0.032 and -0.191 eV·nm² for $e^{S_{11}}$ and $e^{S_{22}}$, respectively, if $j = 2$. To calculate $e^{S_{22}}$ energies, the parameters A_1 and A_2 are 87.4 nm and 613.7. The value of A_3 depends on the SWNT (n, m) chirality. For $j = \text{mod}[(n - m), 3]$, A_3 is 0.143 eV·nm² if $j = 1$; A_3 is -0.191 eV·nm² if $j = 2$. Lastly, θ and d_t are the chiral angle (degree) and diameter (nm), respectively, of each SWNT (n, m) species.

Figure S1. pH-dependent absorption spectra changes of FMN-SWNT dispersion prepared by 1: 4: 4 protocol.

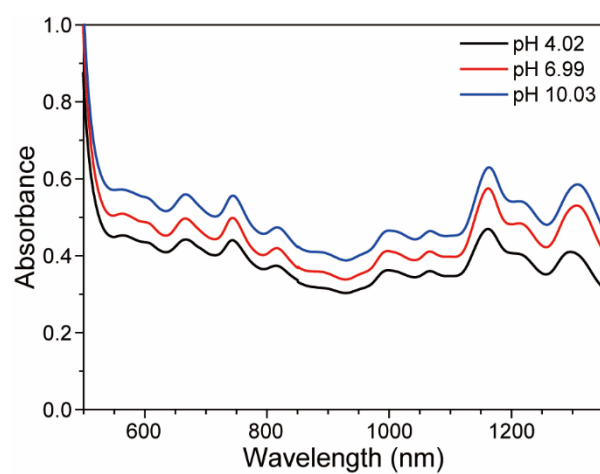


Figure S2. Absorption spectra changes according to different dispersion protocols (1:4:1, 1:4:4, and 1:4:8) and solvents. *1:4:1 protocol:* (A) as-dispersed FC12- and FMN-SWNT dispersions in various solvents and (B) diluted dispersions for PLE maps. *1:4:4 protocol:* (C) as-dispersed FC12- and FMN-SWNT dispersions in various solvents and (D) diluted dispersions for PLE maps. *1:4:8 protocol:* (E) as-dispersed FC12- and FMN-SWNT dispersions in various solvents and (F) diluted dispersions for PLE maps. The absorbance was optionally multiplied according to beam path length.

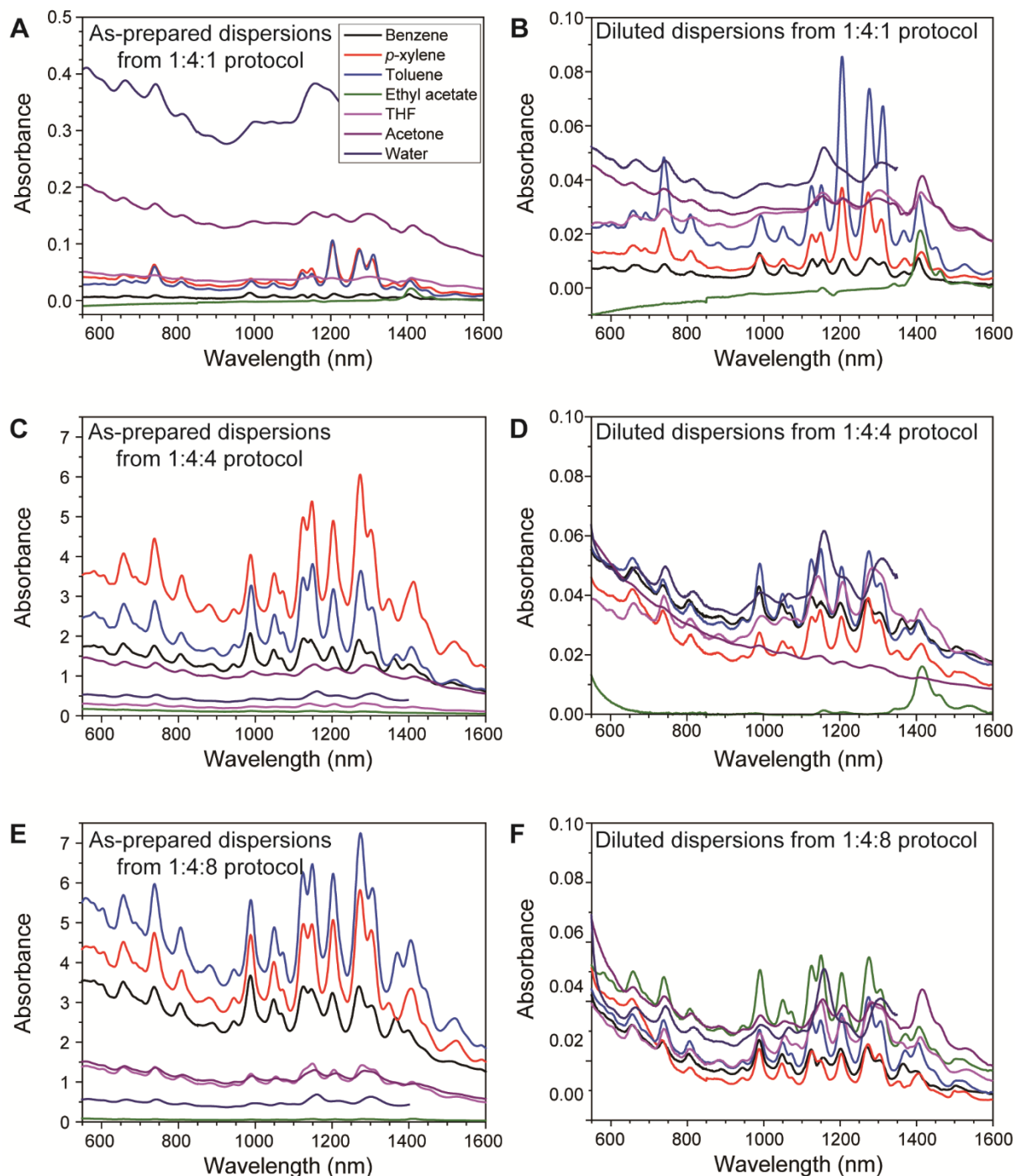


Figure S3. Absorption spectra and PLE maps of flavin-SWNT from 1:4:0.5 and 1:4:0.75 protocols. Data set from 1:4:0.5 protocol: (A) Normalized UV-vis-NIR absorption spectra of FC12-SWNT dispersions in organic solvents and a FMN-SWNT dispersion in water. Normalizations were conducted with respect to the absorbance maximum of $e^{S_{11}}$ near 1270 nm. Each spectrum is offset by 0.6 with increasing ε for visual clarity. Pink shaded area contains absorption from residual water. (B) Corresponding PLE contour maps of SWNT dispersions in various solvents. Rectangular symbols in the first panel indicate crosspoints of $e^{S_{11}}$ and $e^{S_{22}}$. White lines are drawn for the positional comparison of each $e^{S_{11}}$ and $e^{S_{22}}$. Several enriched species are denoted by (n, m) chiralities. Similar (C) absorbance and (D) PLE maps from dispersions with 1:4:0.75 protocol. Asterisk indicates benzene absorption.

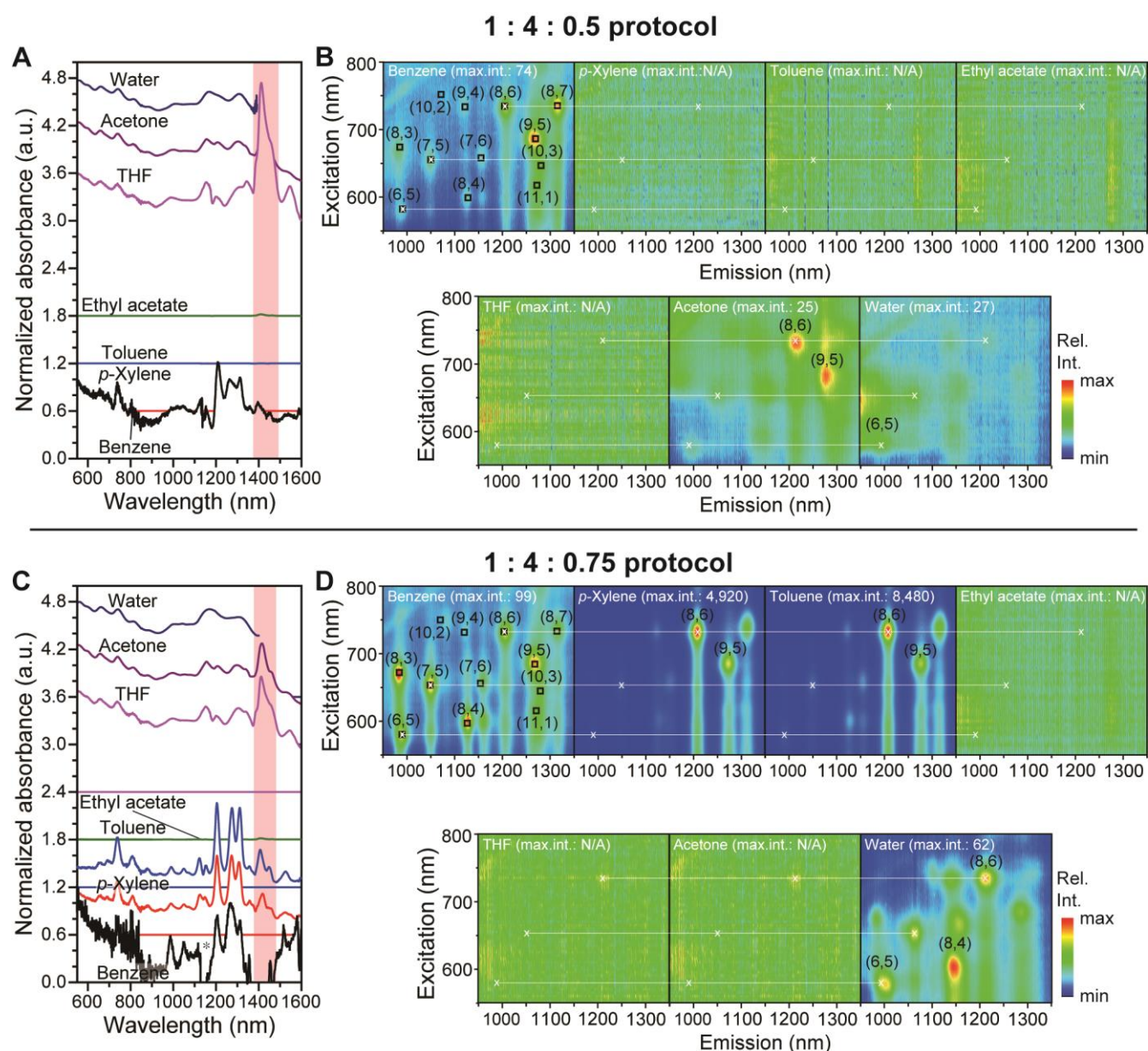


Figure S4. Metallic SWNT content change of FC12-SWNT dispersions in *p*-xylene according to flavin concentration.

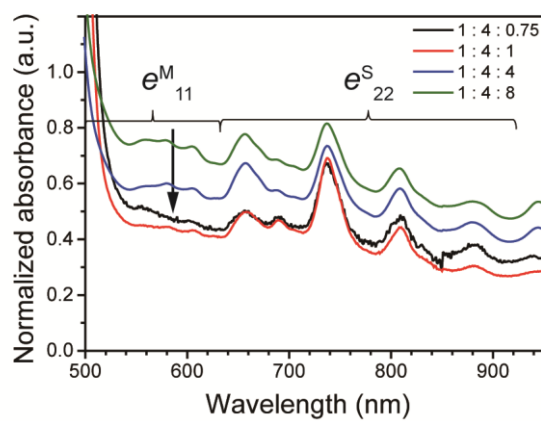
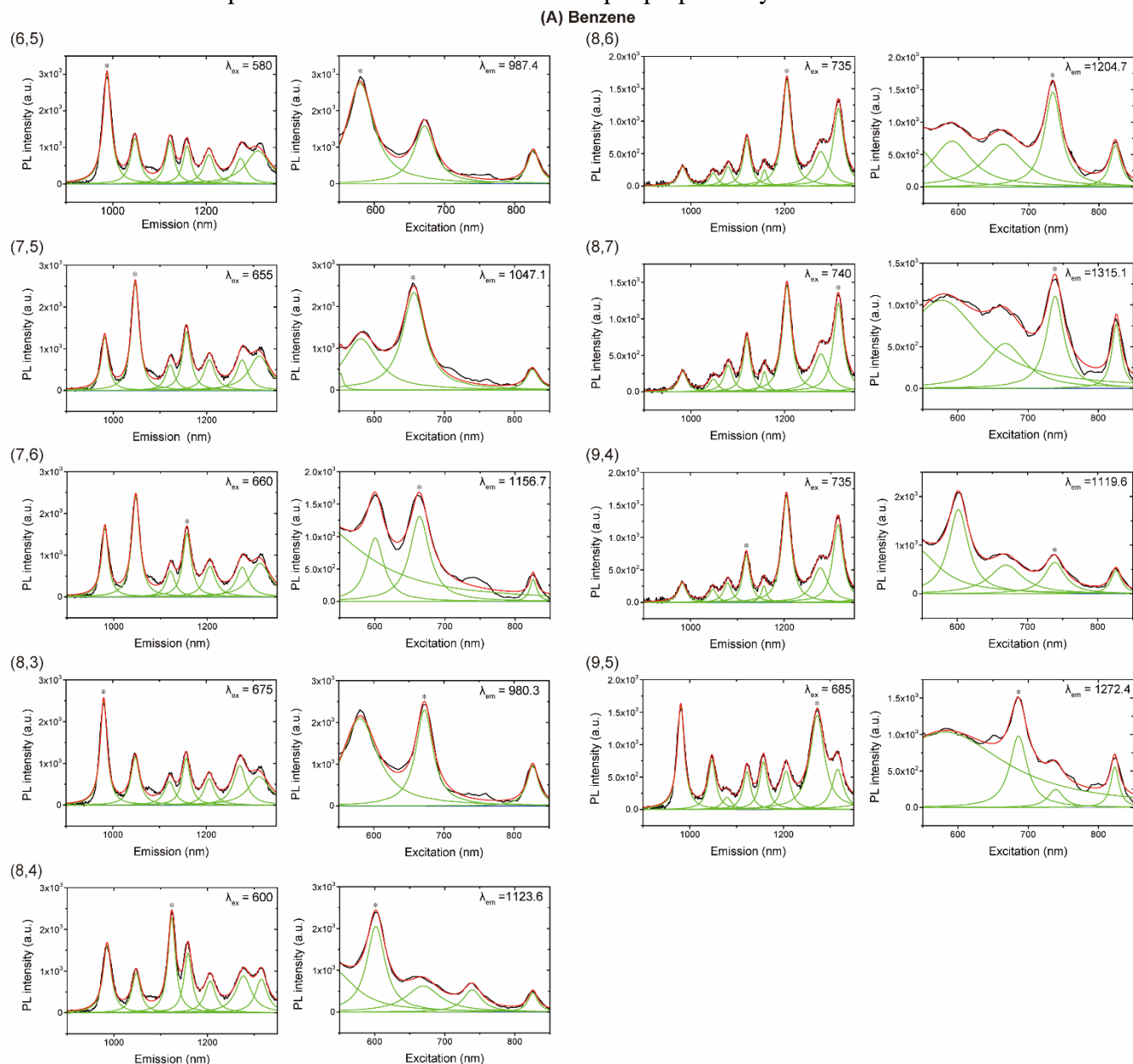


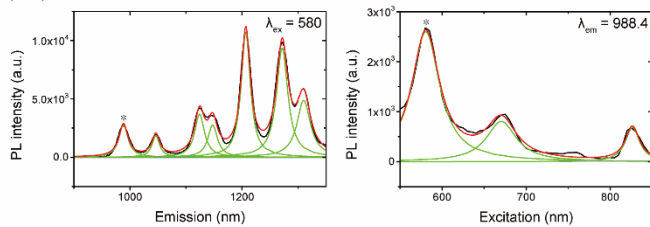
Figure S5. Lorentzian deconvolutions and PL positions determination of SWNT according to solvents. Emission spectra (left) and excitation spectra (right) of nine major SWNT chiralities from (A) benzene, (B) *p*-xylene, (C) toluene, (D) ethyl acetate, (E) THF, (F) acetone, and (G) water. Excitation wavelength (λ_{ex}) and emission wavelength (λ_{em}) are denoted right corner. Asterisk indicates SWNT chirality of interest for deconvolution. Black, green, and red lines indicate original PL data, Lorentzian fitting, and summation of Lorentzian fitting, respectively. Benzene, *p*-xylene, toluene dispersions were obtained from 1:4:1 protocol and ethyl acetate, THF, acetone, and water dispersions were obtained from 1:4:4 protocol. ** These spectra were obtained from the sample prepared by extended sonication for 2 h.



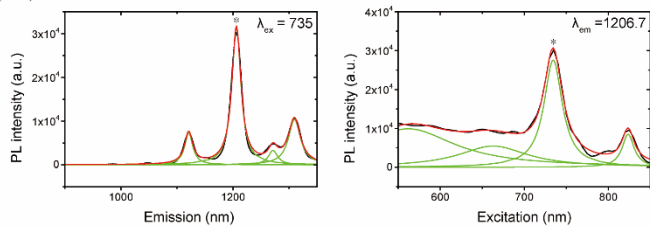
(continued from the previous page)

(B) *p*-Xylene

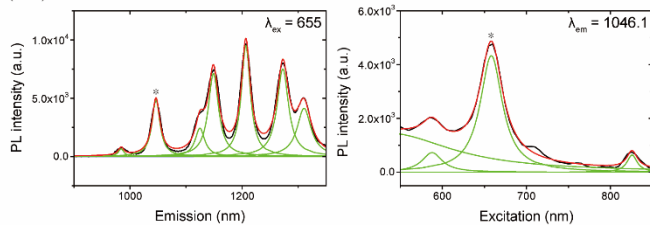
(6,5)



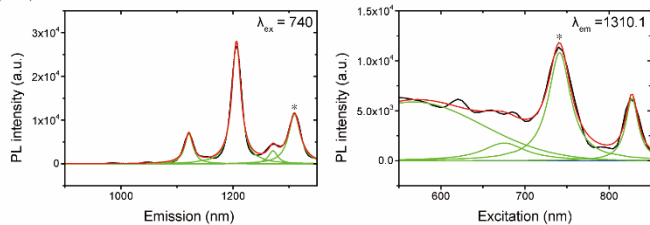
(8,6)



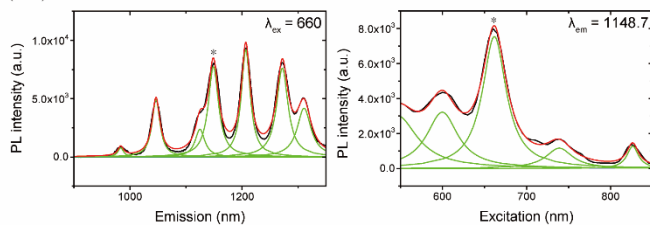
(7,5)



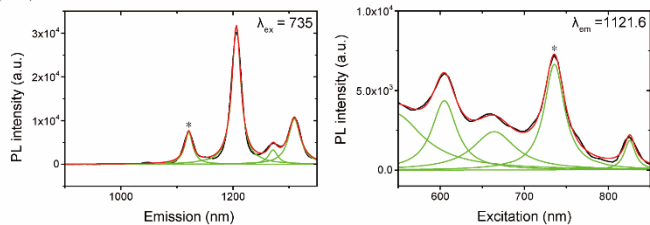
(8,7)



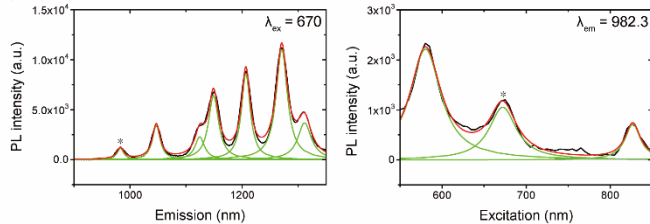
(7,6)



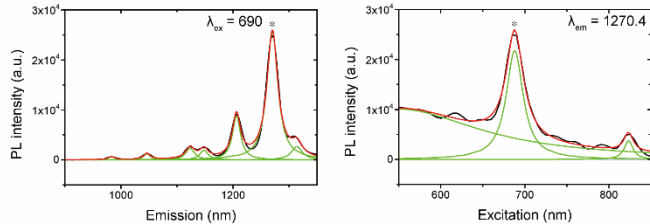
(9,4)



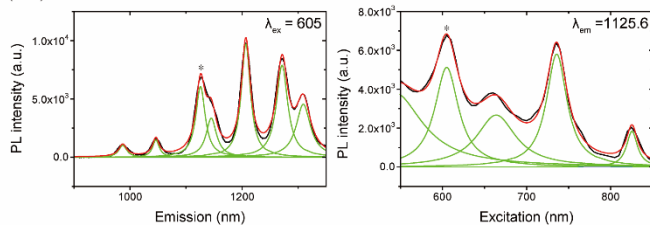
(8,3)



(9,5)

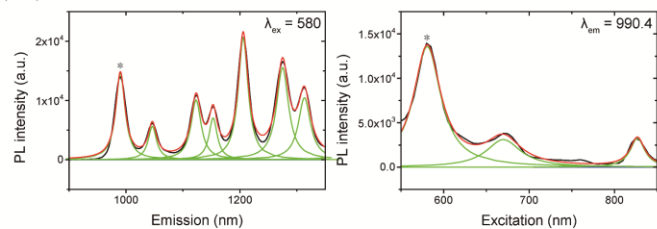


(8,4)

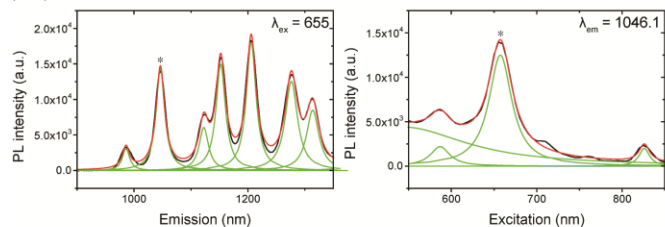


(continued from the previous page)

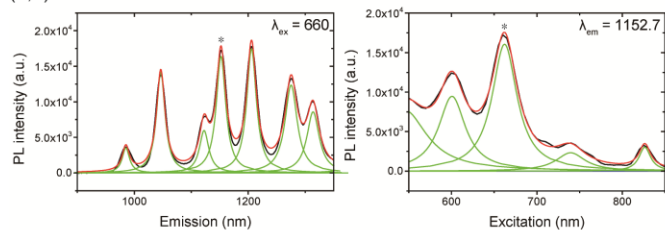
(6,5)



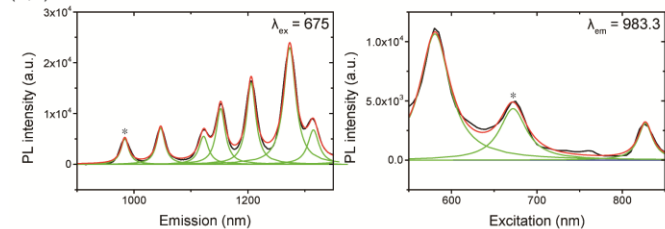
(7,5)



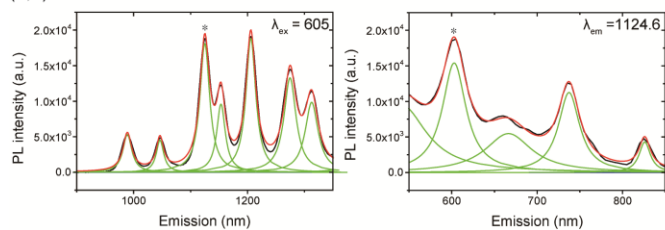
(7,6)



(8,3)

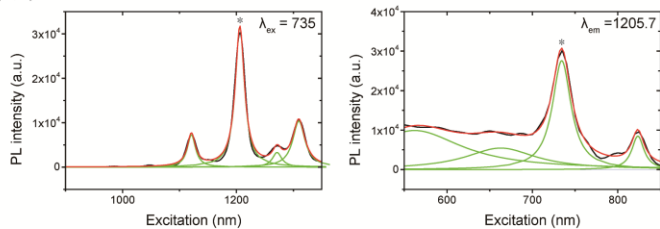


(8,4)

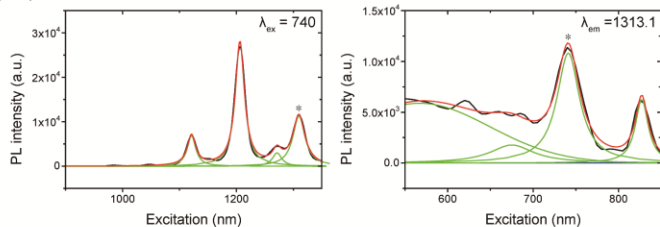


(C) Toluene

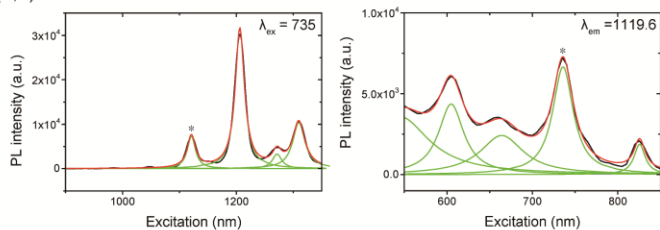
(8,6)



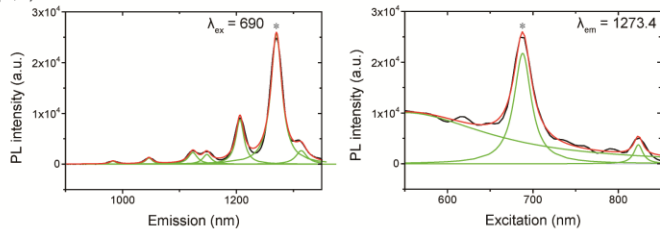
(8,7)



(9,4)



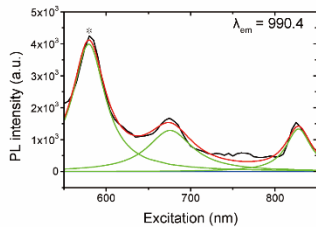
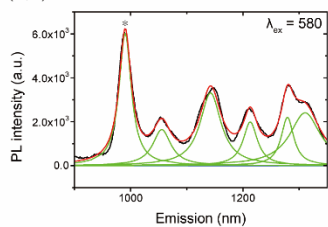
(9,5)



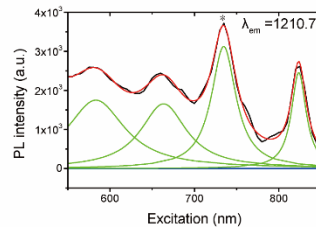
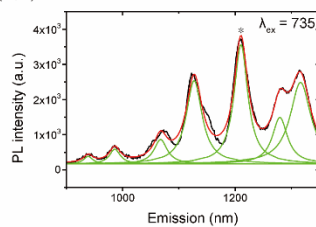
(continued from the previous page)

(D) Ethyl acetate

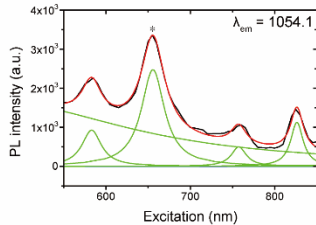
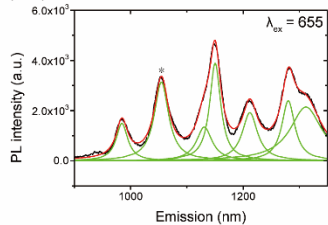
(6,5)



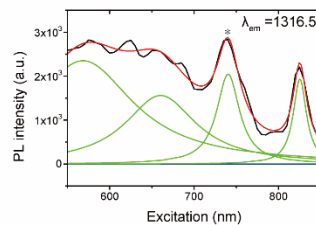
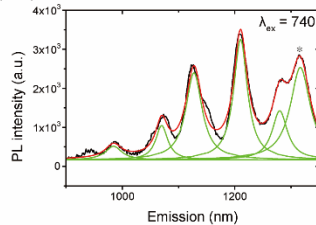
(8,6)



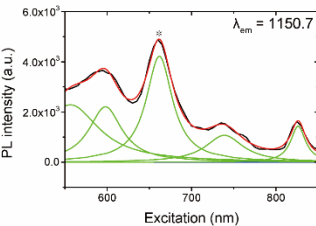
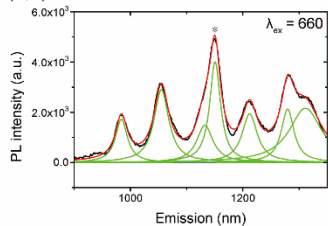
(7,5)



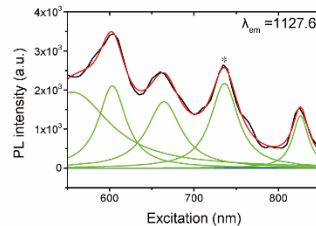
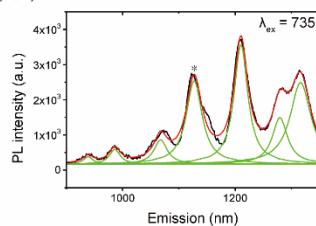
(8,7)



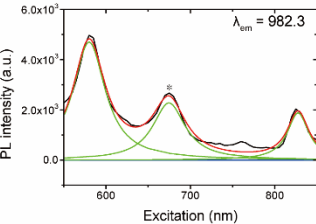
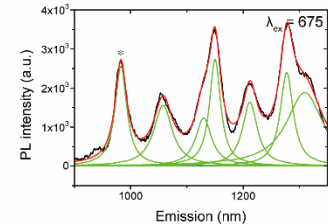
(7,6)



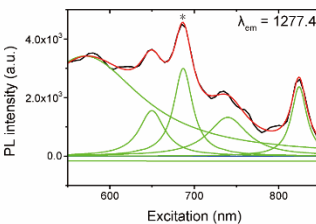
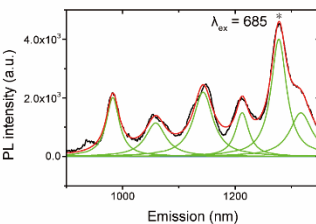
(9,4)



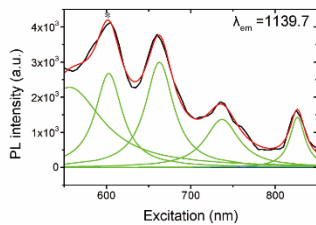
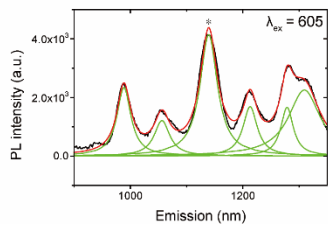
(8,3)



(9,5)

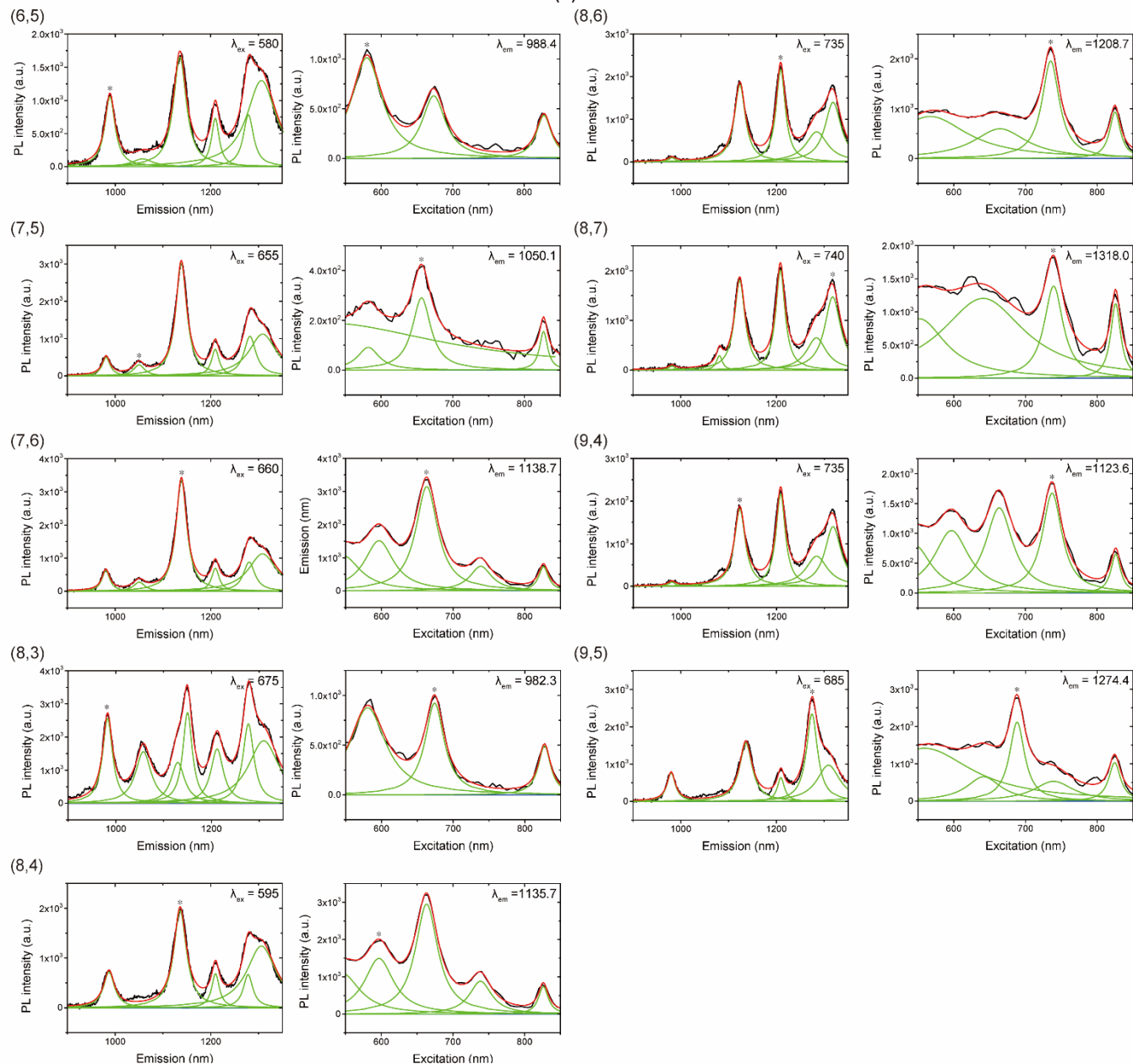


(8,4)



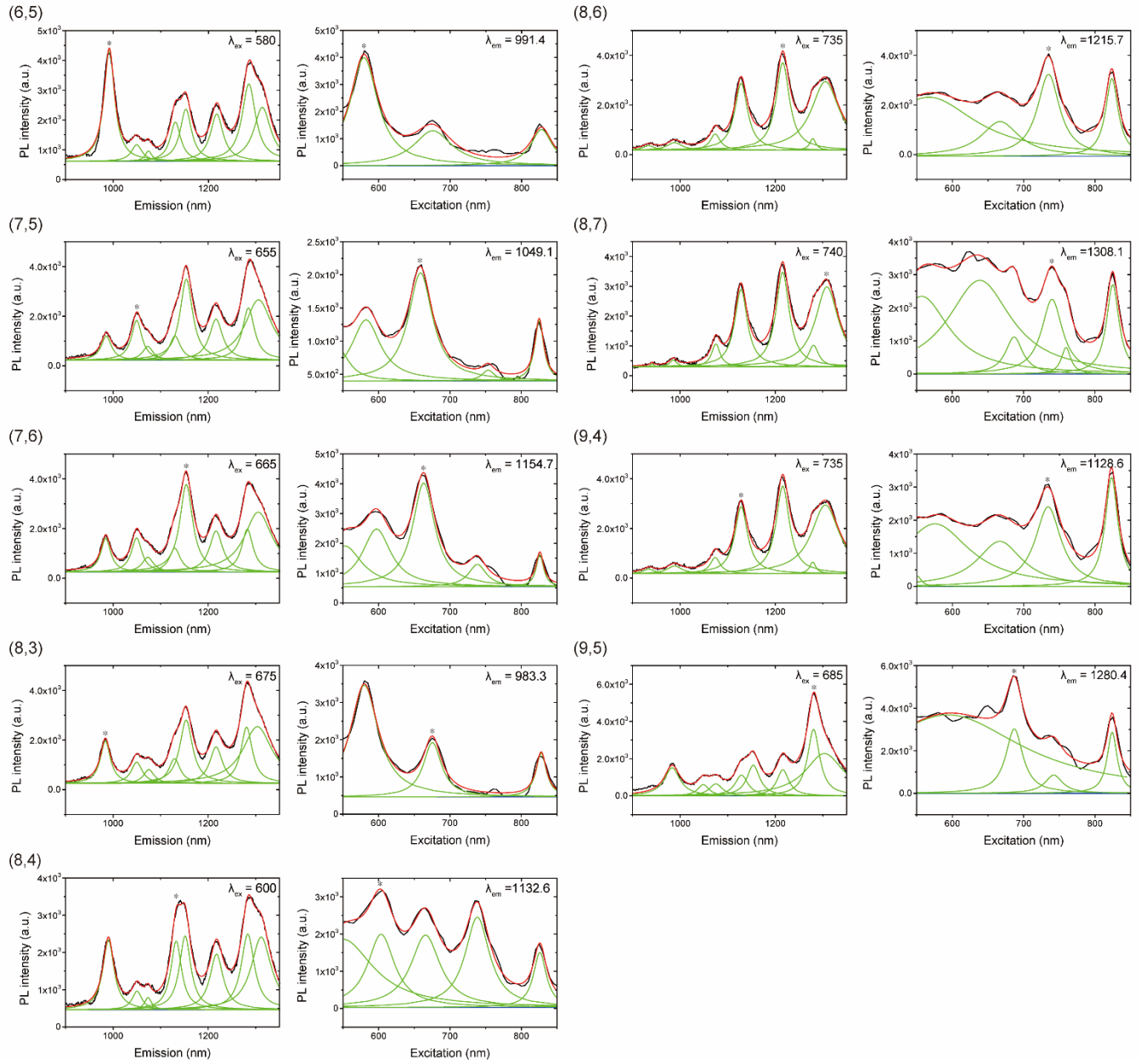
(continued from the previous page)

(E) THF



(continued from the previous page)

(F) Acetone



(continued from the previous page)

(G) Water

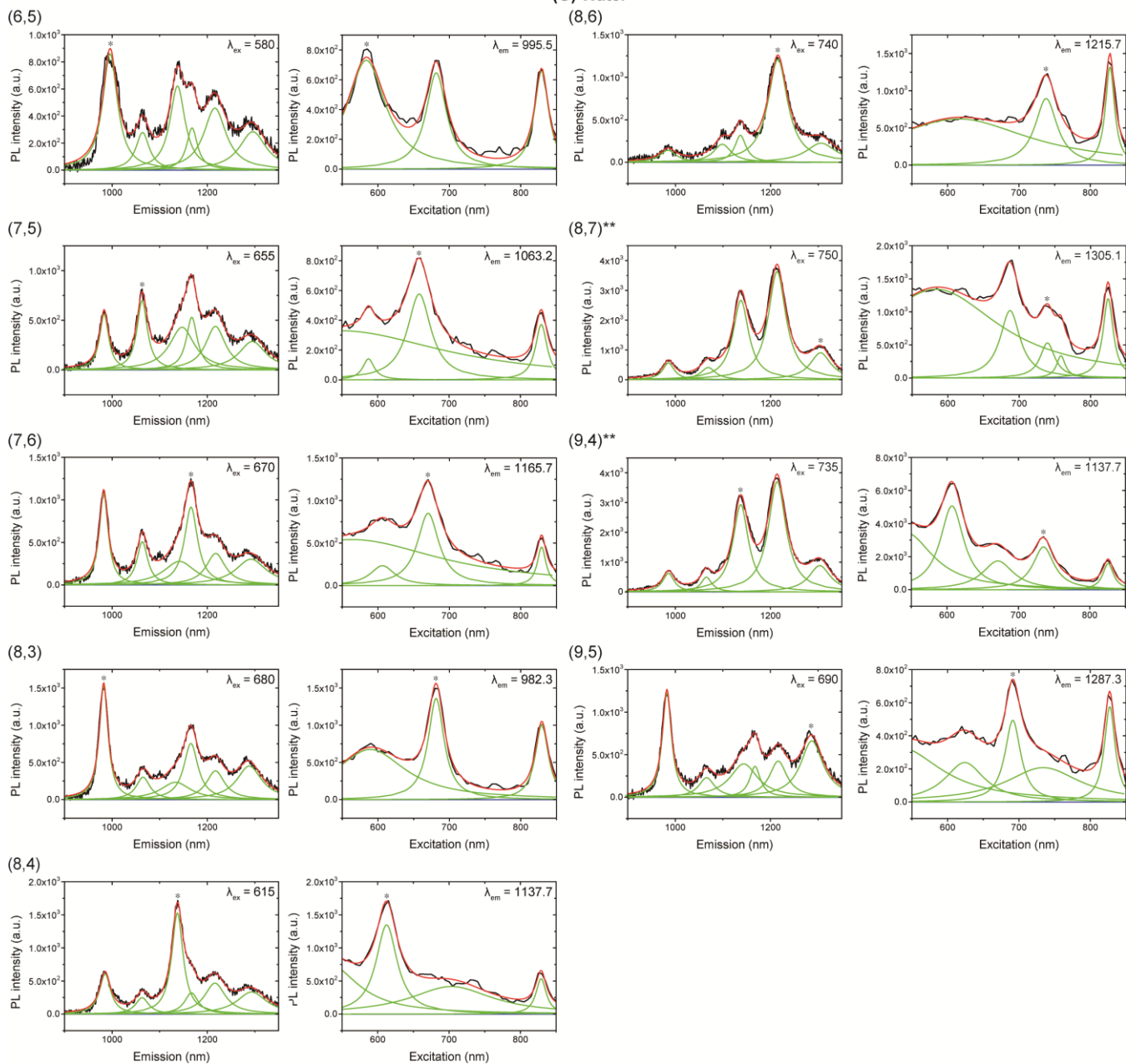


Figure S6. Γ change of (8,6) emission according to dispersion solvents.

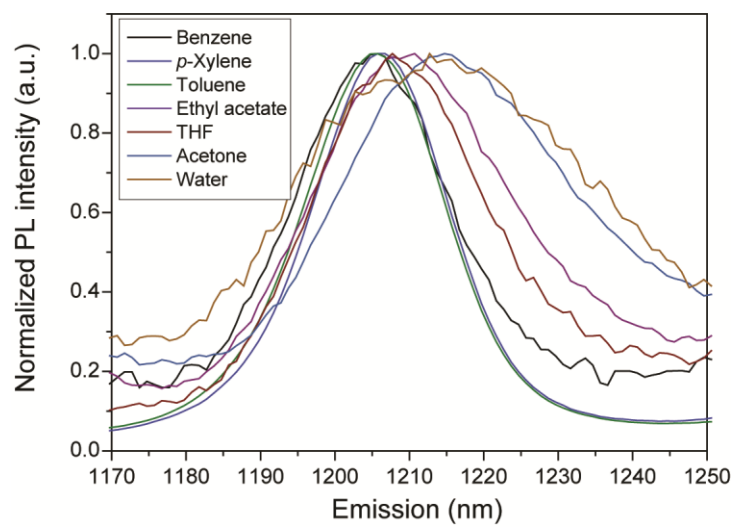


Figure S7. The corresponding AFM phase images from Figure 3.

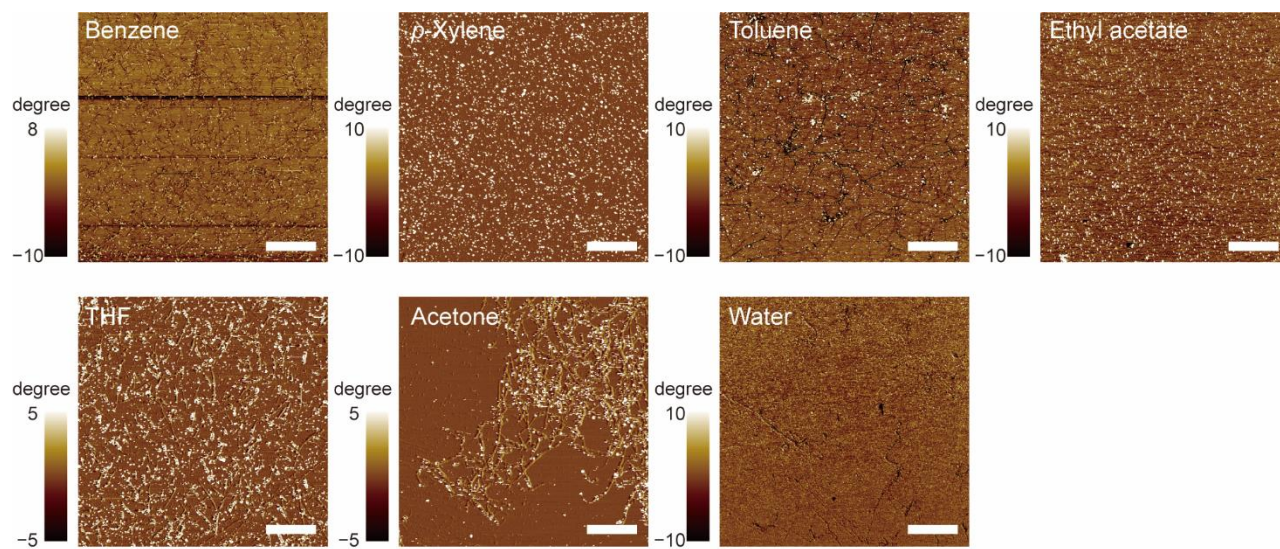


Figure S8. (A to G) Additional AFM topographic images of SWNT dispersions from various solvents. (H) Offset height profiles from each sample. Gray lines were drawn to indicate height limit of a iSWNT wrapped by flavins.

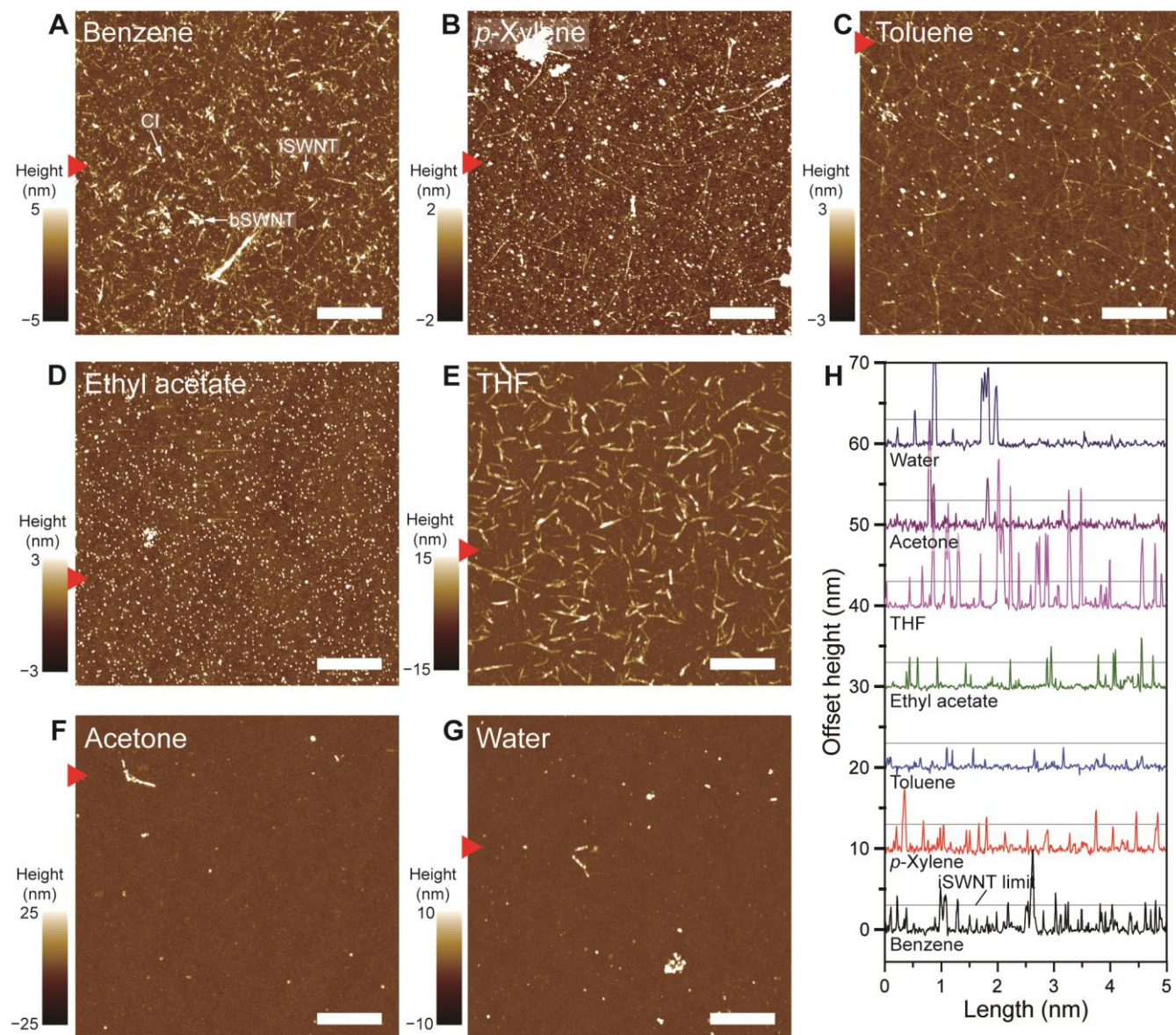


Figure S9. (A) AFM height and (B) phase images of representative individualized HiPco SWNT wrapped by FC12 deposited on SiO₂/Si substrate. Sample was prepared by dispersion in toluene. (C) Height trace of FC12-wrapped SWNT as indicated by pair of triangles in (A). Undulation originates from FC12 wrapping.

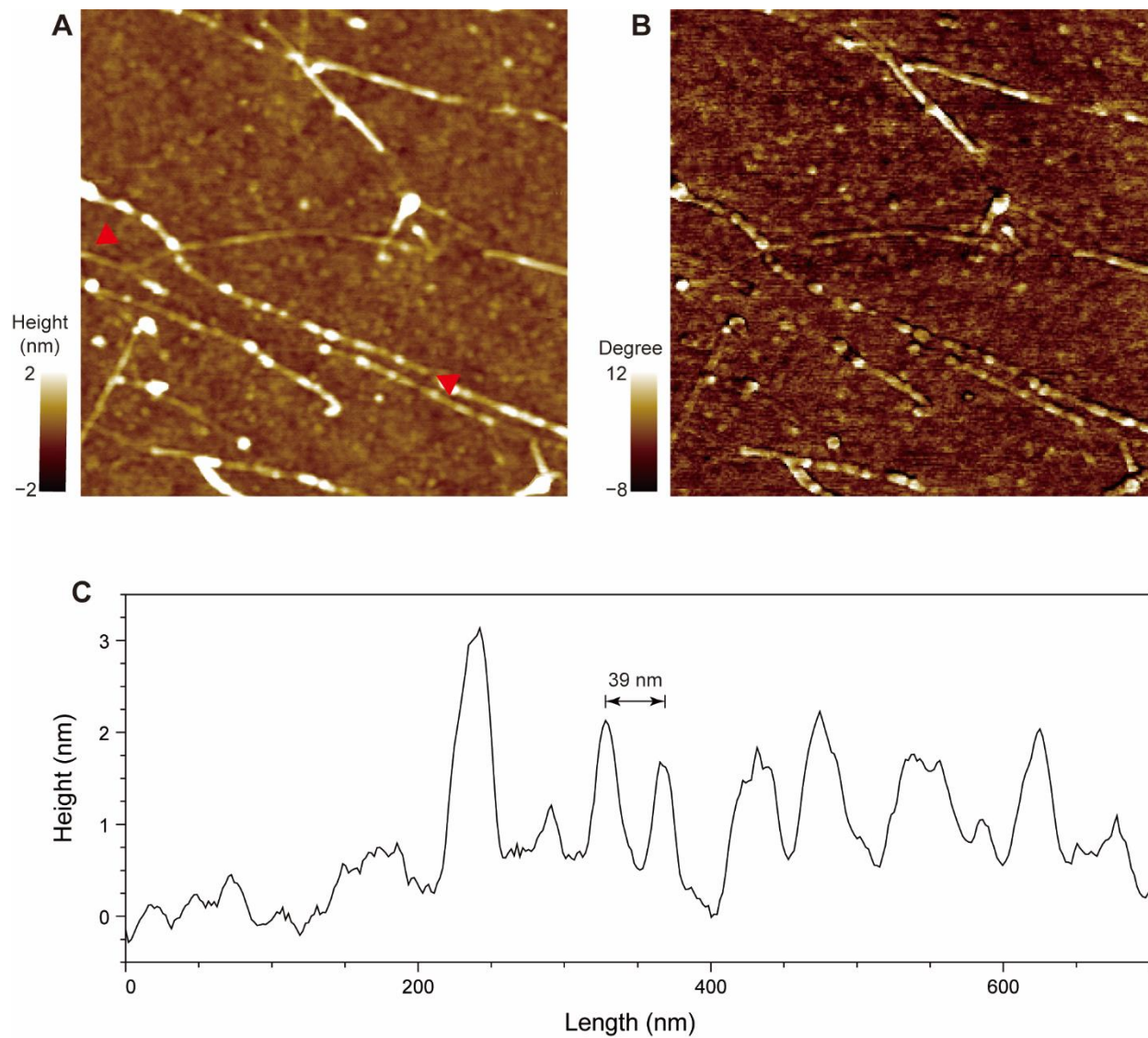


Figure S10. (A to F) Absorbance (left) and PL emission (right) spectra measurements for Φ_R of (7,6) from each SWNT dispersion. (left) Diluted absorbances and its analytical contributions from SWNT (α) and background (β) to obtain net absorbance. (right) PL emission spectra containing maximum I_{PL} of (7,6).

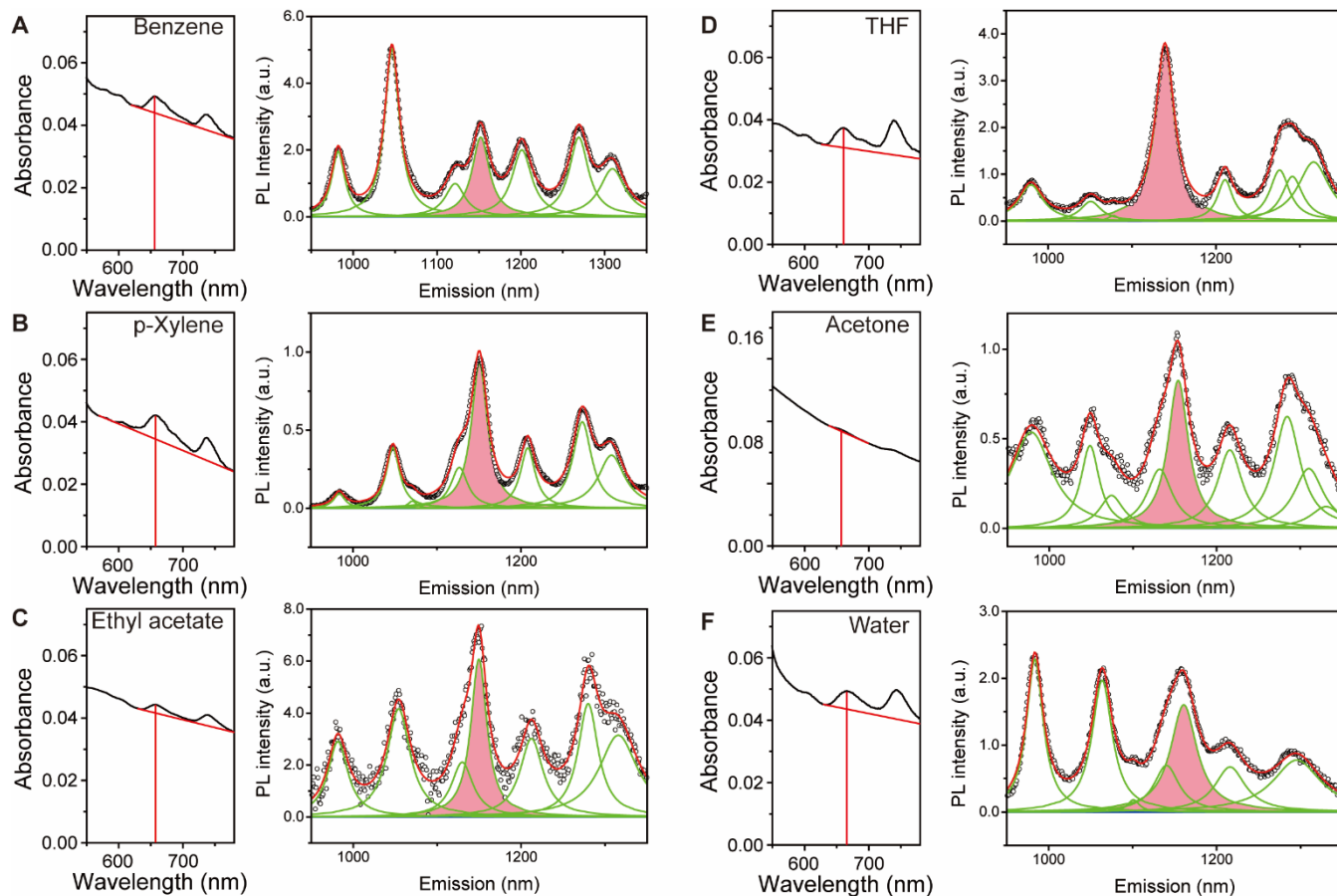


Figure S11. (A) HOMO and LUMO levels of lumiflavin and (B) energy gap depending on solvents.

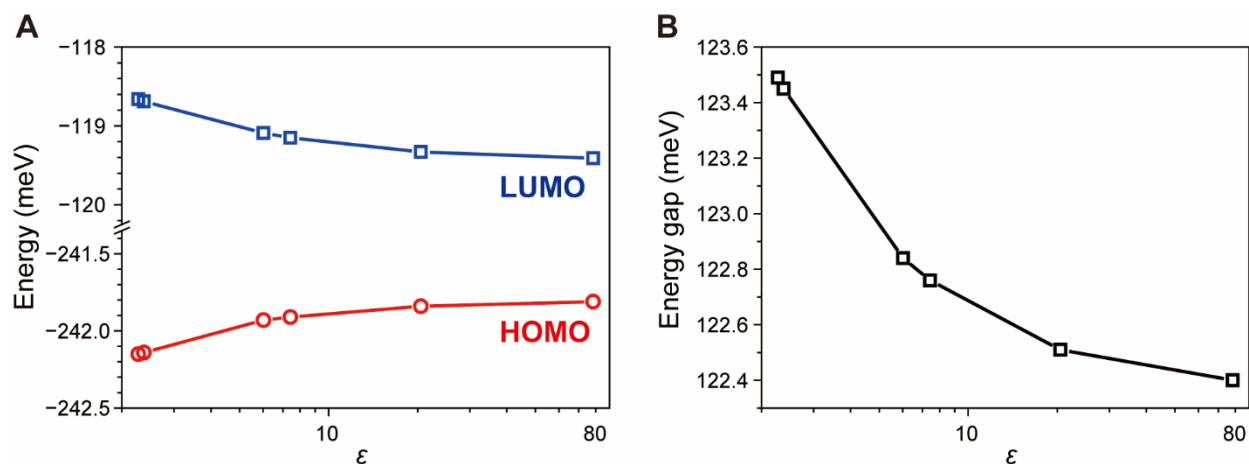


Figure S12. Normalized absorption spectra changes of FC12 and FMN in various solvents.

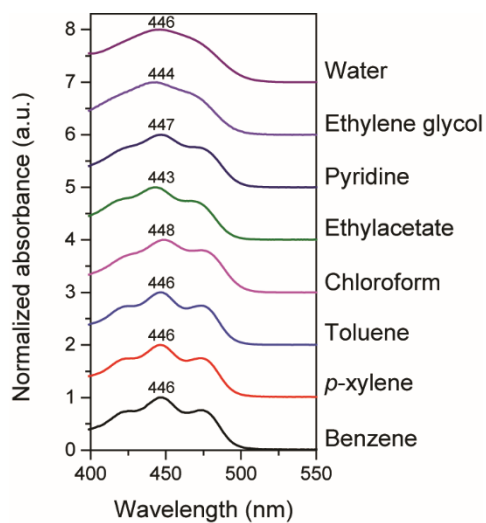


Figure S13. Comparison of Figure 7B with data from reference S4 and S5. Δe_{11}^S trends of (A) flavin-SWNT and (B) SDS-SWNT. Both data are normalized with benzene cases.

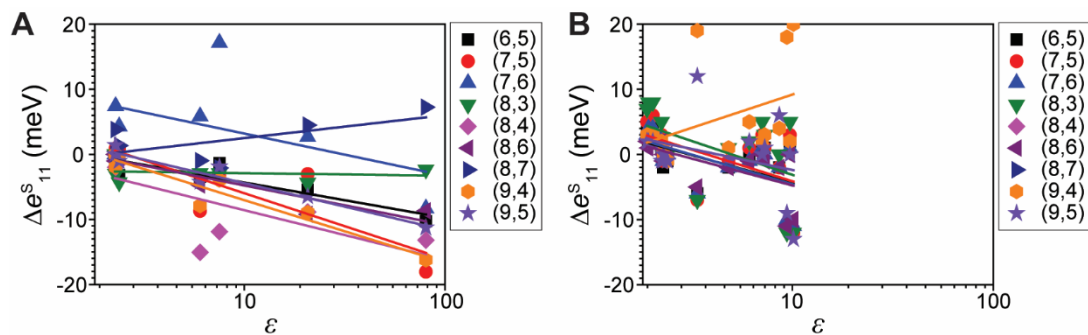


Table S1. ϵ , solubility, δ , and δ subcomponents of the used solvents in this study.

Solvent	ϵ^{\ast}	FC12		Lumiflavin	δ^{\ast} (MPa ^{1/2})	δ_D (MPa ^{1/2})	δ_P (MPa ^{1/2})	δ_H (MPa ^{1/2})
		Solubility [§] (mg/mL)	λ_{\max} (nm)	Solubility [§] (μ g/mL)				
Water	80.4	N/A	444	N/A	47.9-48.1	12.3-14.3	31.3	34.2
Ethylene glycol [‡]	41.4	0.1	443	N/A	29.1-33.4	20.6	16.9	11.1
Acetonitrile [‡]	37.5	N/A	N/A	N/A	24.1-24.5	15.4-16.2	18	6.1
Methanol [‡]	33.6	4.72	443	N/A	27.2-29.7	18.7-19.8	15.2	12.3
Acetone	20.7 [*]	1.81	443	53.9	20.0-20.5	15.5	10.4	7
Pyridine [‡]	12.3 [*]	70.38	447	528.7	21.7-21.9	18.9-20.1	8.8	5.9
Methylenechloride	9.08	34.90	446	N/A	19.9	17.4-18.2	6.4	6.1
THF	7.52 [*]	11.03	444	46.2	19.5	16.8-18.9	5.7	8
Ethyl acetate	6.02 [*]	0.51	443	14.1	18.6	15.2	5.3	9.2
Chloroform [‡]	4.81	58.0	448	N/A	18.9-19.0	17.7-18.1	3.1	5.7
Toluene	2.38 [*]	0.23	446	4.3	18.2-18.3	17.3-18.1	1.4	2
Benzene	2.28	0.31	446	4.4	18.5-18.8	17.3-18.5	1	2
<i>p</i> -Xylene	2.27	0.25	446	N/A	17.9-18.0	16.6-17.3	1	1

※ ϵ values were obtained from reference S⁶ at 20 °C.

§ Some of the solubilities were obtained from reference S⁷.

‡ These solvents gave SWNT dispersions that do not have PL activities.

♣ δ and their subcomponents were obtained from reference S2.

* Values are obtained at 25 °C except THF measured at 22 °C.

Table S2. SWNT chiralities and their deconvoluted $e^{S_{11}}$, $e^{S_{22}}$, and Γ dispersed in various media.

(n,m)	d_t (nm)	Benzene				<i>p</i> -Xylene				Toluene				Ethyl acetate			
		$e^{S_{11}}$ (nm)	$e^{S_{22}}$ (nm)	Emission Γ (meV)	PL intensity (a.u.)	$e^{S_{11}}$ (nm)	$e^{S_{22}}$ (nm)	Emission Γ (meV)	PL intensity (a.u.)	$e^{S_{11}}$ (nm)	$e^{S_{22}}$ (nm)	Emission Γ (meV)	PL intensity (a.u.)	$e^{S_{11}}$ (nm)	$e^{S_{22}}$ (nm)	Emission Γ (meV)	PL intensity (a.u.)
(6,5)	0.76	987.6	580.2	26.8	701.7	988.4	580.5	24.8	776	990.2	580.8	24.9	2749.2	987.6	580.2	26.8	21.0
(7,5)	0.83	1047.1	656.4	22.9	561.1	1046.3	658.2	19.5	805.8	1046.3	657.4	20.6	1933.2	1047.1	656.4	22.9	10.8
(7,6)	0.89	1156.9	663.7	23.3	281.3	1148.9	661.7	20.8	1920.4	1152.3	662.2	20.5	3247.0	1156.9	663.7	23.3	15.0
(8,3)	0.78	980.5	672.1	22.9	132.0	982.9	672.2	18.7	264	983.9	672.1	21.4	754.8	980.5	672.1	22.9	9.0
(8,4)	0.84	1123.7	601.7	19.1	380.2	1125.8	605.0	19.8	1166.6	1125.0	602.8	20.3	1994.6	1123.7	601.7	19.1	13.8
(8,6)	0.97	1204.9	734.5	20.0	551.2	1206.1	734.2	16.9	2479.8	1205.3	737.4	17.2	3629.4	1204.9	734.5	20.0	13.2
(8,7)	1.03	1315.1	738.7	18.5	386.3	1309.8	741.2	18.5	1777.4	1313.2	740.7	17.8	1689.8	1315.1	738.7	18.5	10.4
(9,4)	0.92	1119.2	738.9	18.8	180.1	1121.2	735.8	23.9	1648.6	1119.7	737.0	16.6	2369.4	1119.2	738.9	18.8	10.1
(9,5)	0.98	1272.2	686.3	28.0	596.1	988.4	580.5	24.8	776	990.2	580.8	24.9	2749.2	1272.2	686.3	28.0	16.3

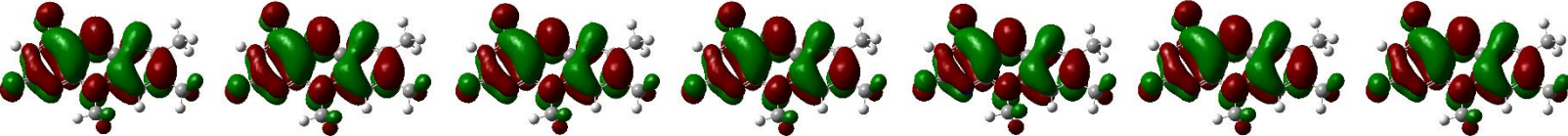
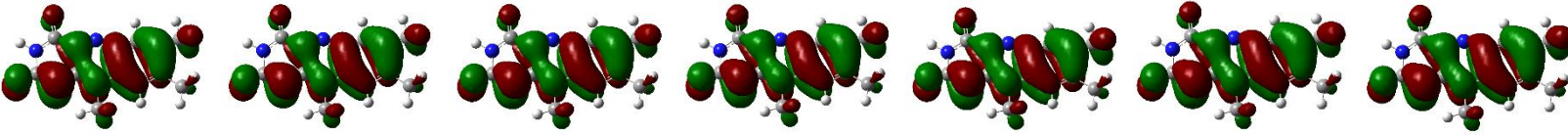
(n,m)	d_t (nm)	THF				Acetone				Water				Spread in $e^{S_{11}}$ (meV) among solvents	Spread in $e^{S_{22}}$ (meV) among solvents
		$e^{S_{11}}$ (nm)	$e^{S_{22}}$ (nm)	Emission Γ (meV)	PL intensity (a.u.)	$e^{S_{11}}$ (nm)	$e^{S_{22}}$ (nm)	Emission Γ (meV)	PL intensity (a.u.)	$e^{S_{11}}$ (nm)	$e^{S_{22}}$ (nm)	Emission Γ (meV)	PL intensity (a.u.)		
(6,5)	0.76	988.4	580.5	24.8	78.8	990.2	580.8	24.9	35.6	995.8	583.6	47.2	121.2	10.3	13.9
(7,5)	0.83	1046.3	658.2	19.5	32.2	1046.3	657.4	20.6	13.8	1063.3	658.2	29.0	319.5	19.0	8.6
(7,6)	0.89	1148.9	661.7	20.8	184.2	1152.3	662.2	20.5	21.8	1165.9	670.3	30.6	214.2	25.5	23.9
(8,3)	0.78	982.9	672.2	18.7	59.4	983.9	672.1	21.4	14.82	982.3	681.5	28.4	265.7	4.4	25.4
(8,4)	0.84	1125.8	605.0	19.8	114.3	1125.0	602.8	20.3	18.68	1137.3	606.9	27.7	329.9	15.1	34.2
(8,6)	0.97	1206.1	734.2	16.9	127.3	1205.3	737.4	17.2	19.4	1215.1	738.1	41.9	179.8	9.2	8.8
(8,7)	1.03	1309.8	741.2	18.5	121.0	1313.2	740.7	17.8	14.0	1305.1	739.6	38.8	72.3	9.3	5.8
(9,4)	0.92	1121.2	735.8	23.9	104.4	1119.7	737.0	16.6	15.1	1137.4	735.2	53.8	169.8	17.7	10.7
(9,5)	0.98	1270.4	688.0	18.0	168.9	1273.5	688.4	18.9	23.6	1287.0	691.4	43.0	137.5	12.6	13.4

Table S3. Φ_R calculations of (7,6) chirality according to solvent.

Solvent	Absorbance		PL intensity area (I_{PL}) near certain wavelength (nm)									$I_{PL,(7,6)} / \sum I_{PL}$ (%)	$\alpha_{(7,6)}$ ($\times 10^{-4}$)	$I_{PL,(7,6)} / \alpha_{(7,6)}$	n_s^*	Norm. Φ_R	
	α	β	985	1050	1070	1121	1150	1201	1270	1291	1309					$n = 1$	$n = n_s$
Benzene	0.0053	0.0440	5890	16888	N/A	4491	9311	9041	10388	N/A	8322	0.14	8	12181052	1.50	1.000	2.253
<i>p</i> -Xylene	0.0075	0.0346	4806	23771	1806	47175	67497	25991	47175	N/A	40982	0.26	20	34499314	1.50	2.832	6.346
Toluene	0.0078	0.0447	16425	55077	6201	27457	109068	N/A	61360	N/A	35599	0.35	27	39741375	1.49	3.263	7.300
Ethyl acetate	0.0028	0.1454	265	434	N/A	N/A	441	315	400	N/A	552	0.18	5	868765	1.37	0.071	0.134
THF	0.0067	0.0307	2120	987	131	N/A	8088	1539	2456	2268	4488	0.37	24	3317142	1.40	0.272	0.537
Acetone	0.0020	0.1287	1013	393	200	381	763	497	746	N/A	453	0.17	4	2176792	1.36	0.179	0.329
Water	0.0059	0.0436	2928	3026	3200	166	1332	1555	2838	N/A	N/A	0.09	5	2543114	1.33	0.209	0.370

* n_s values were measured at 25 °C, obtained from reference S⁸. n_s value of ethyl acetate was obtained from reference S⁹.

Table S4. Isoelectric contours of LUMO and HOMO and respective energy levels of lumiflavin in various solvents. Note that ϵ listed in table uses values in Gaussian program.

Energy level		Solvents (ϵ)						
		<i>p</i> -Xylene (2.27)	Benzene (2.27)	Toluene (2.37)	Ethylacetate (6.02)	THF (7.43)	Acetone (20.50)	Water (78.36)
LUMO	Isoelectric contour							
	eV	-0.1187	-0.1187	-0.1187	-0.1191	-0.1192	-0.1193	-0.1194
HOMO	Isoelectric contour							
	eV	-0.2422	-0.2422	-0.2421	-0.2419	-0.2419	-0.2418	-0.2418

Cited references

- S1. Pfohl, M.; Tune, D. D.; Graf, A.; Zaumseil, J.; Krupke, R.; Flavel, B. S., Fitting Single-Walled Carbon Nanotube Optical Spectra. *ACS Omega* **2017**, 2 (3), 1163-1171.
2. Krevelen, D. W. V., *Properties of Polymers*. 3rd Edition ed.; Elsevier, Press, Amsterdam: Amsterdam, 1990; p 203.
3. Choi, J. H.; Strano, M. S., Solvatochromism in Single-Walled Carbon Nanotubes. *Appl. Phys. Lett.* **2007**, 90 (22), 223114.
4. Zheng, M.; Jagota, A.; Strano, M. S.; Santos, A. P.; Barone, P.; Chou, S. G.; Diner, B. A.; Dresselhaus, M. S.; Mclean, R. S.; Onoa, G. B.; Samsonidze, G. G.; Semke, E. D.; Usrey, M.; Walls, D. J., Structure-Based Carbon Nanotube Sorting by Sequence-Dependent DNA Assembly. *Science* **2003**, 302 (5650), 1545-1548.
5. Silvera-Batista, C. A.; Wang, R. K.; Weinberg, P.; Ziegler, K. J., Solvatochromic Shifts of Single-Walled Carbon Nanotubes in Nonpolar Microenvironments. *Phys. Chem. Chem. Phys.* **2010**, 12 (26), 6990-6998.
6. Maryott, A. A.; Smith, E. R., *Table of Dielectric Constants of Pure Liquids*. National Bureau of Standards: Washington, D.C., 1951; Vol. 514.
7. Ju, S.-Y.; Kopcha, W. P.; Papadimitrakopoulos, F., Brightly Fluorescent Single-Walled Carbon Nanotubes *via* an Oxygen-Excluding Surfactant Organization. *Science* **2009**, 323 (5919), 1319-1323.
8. Saunders, J. E.; Sanders, C.; Chen, H.; Loock, H.-P., Refractive Indices of Common Solvents and Solutions at 1550 nm. *Appl. Opt.* **2016**, 55 (4), 947-953.
9. Kell, G. S., Precise Representation of Volume Properties of Water at One Atmosphere. *J. Chem. Eng. Data* **1967**, 12 (1), 66-69.